



**HAL**  
open science

## Characterisation of adipocyte-derived extracellular vesicle subtypes identifies distinct protein and lipid signatures for large and small extracellular vesicles

Maëva Durcin, Audrey Fleury, Emiliane Taillebois, Grégory Hilairet, Zuzana Krupova, Celine Henry, Sandrine Truchet, Martin Trötz Müller, Harald Köfeler, Guillaume Mabileau, et al.

### ► To cite this version:

Maëva Durcin, Audrey Fleury, Emiliane Taillebois, Grégory Hilairet, Zuzana Krupova, et al.. Characterisation of adipocyte-derived extracellular vesicle subtypes identifies distinct protein and lipid signatures for large and small extracellular vesicles. *Journal of Extracellular Vesicles*, 2017, 6 (1), pp.1-23. 10.1080/20013078.2017.1305677 . hal-01606680

**HAL Id: hal-01606680**

**<https://hal.science/hal-01606680>**

Submitted on 29 May 2024

**HAL** is a multi-disciplinary open access archive for the deposit and dissemination of scientific research documents, whether they are published or not. The documents may come from teaching and research institutions in France or abroad, or from public or private research centers.

L'archive ouverte pluridisciplinaire **HAL**, est destinée au dépôt et à la diffusion de documents scientifiques de niveau recherche, publiés ou non, émanant des établissements d'enseignement et de recherche français ou étrangers, des laboratoires publics ou privés.

ARTICLE



## Characterisation of adipocyte-derived extracellular vesicle subtypes identifies distinct protein and lipid signatures for large and small extracellular vesicles

Maëva Durcin<sup>a,b\*</sup>, Audrey Fleury<sup>a\*</sup>, Emiliane Taillebois<sup>a</sup>, Grégory Hilairet<sup>a</sup>, Zuzana Krupova<sup>c,d</sup>, Céline Henry<sup>e</sup>, Sandrine Truchet<sup>b</sup>, Martin Trötz Müller<sup>f,g</sup>, Harald Köfeler<sup>f,g</sup>, Guillaume Mabilieu<sup>h</sup>, Olivier Hue<sup>b</sup>, Ramaroson Andriantsitohaina<sup>a</sup>, Patrice Martin<sup>c</sup> and Soazig Le Lay<sup>a</sup>

<sup>a</sup>INSERM U1063, Oxidative stress and metabolic pathologies, Angers University, Pointe à Pitre, France; <sup>b</sup>Adaptation to Tropical Climate and Exercise Laboratory, EA3596, University of the French West Indies, Pointe-à-Pitre, Guadeloupe, France; <sup>c</sup>GABI, INRA, AgroParisTech, Université Paris-Saclay, Jouy-en-Josas, France; <sup>d</sup>EXCILONE, Elancourt, France; <sup>e</sup>MICALIS Institute, INRA, AgroParisTech, PAPPSSO, Université Paris-Saclay, Jouy-en-Josas, France; <sup>f</sup>Center for Medical Research, Medical University of Graz, Graz, Austria; <sup>g</sup>Omic Center Graz, Graz, Austria; <sup>h</sup>SCIAM, Angers University, Angers, France

### ABSTRACT

Extracellular vesicles (EVs) are biological vectors that can modulate the metabolism of target cells by conveying signalling proteins and genomic material. The level of EVs in plasma is significantly increased in cardiometabolic diseases associated with obesity, suggesting their possible participation in the development of metabolic dysfunction. With regard to the poor definition of adipocyte-derived EVs, the purpose of this study was to characterise both qualitatively and quantitatively EVs subpopulations secreted by fat cells. Adipocyte-derived EVs were isolated by differential centrifugation of conditioned media collected from 3T3-L1 adipocytes cultured for 24 h in serum-free conditions. Based on morphological and biochemical properties, as well as quantification of secreted EVs, we distinguished two subpopulations of adipocyte-derived EVs, namely small extracellular vesicles (sEVs) and large extracellular vesicles (lEVs). Proteomic analyses revealed that lEVs and sEVs exhibit specific protein signatures, allowing us not only to define novel markers of each population, but also to predict their biological functions. Despite similar phospholipid patterns, the comparative lipidomic analysis performed on these EV subclasses revealed a specific cholesterol enrichment of the sEV population, whereas lEVs were characterised by high amounts of externalised phosphatidylserine. Enhanced secretion of lEVs and sEVs is achievable following exposure to different biological stimuli related to the chronic low-grade inflammation state associated with obesity. Finally, we demonstrate the ability of primary murine adipocytes to secrete sEVs and lEVs, which display physical and biological characteristics similar to those described for 3T3-L1. Our study provides additional information and elements to define EV subtypes based on the characterisation of adipocyte-derived EV populations. It also underscores the need to distinguish EV subpopulations, through a combination of multiple approaches and markers, since their specific composition may cause distinct metabolic responses in recipient cells and tissues.

### ARTICLE HISTORY

Received 22 December 2016

### RESPONSIBLE EDITOR

Willem Stoorvogel  
Universiteit Utrecht  
Netherlands

### KEYWORDS



Extracellular vesicles;  
exosomes; microvesicles;  
large EVs; small EVs;  
adipocytes

## Introduction


Obesity has reached epidemic proportions and constitutes a major cause of co-morbidities including type 2 diabetes, cardiovascular diseases and various cancers. Because of its adipocyte lipid storage capacities, white adipose tissue (WAT) constitutes the main energy supply in the body, being mobilised according to the body's needs and therefore implying a state of permanent communication with other organs in the body. However, adipocytes are not restricted to a fat-storage capacity, but can secrete many adipokines that mediate cell

signalling in an autocrine or a paracrine manner. Secretion of these different signalling mediators is often dysregulated with obesity and contributes to a low-grade inflammatory state associated with obesity; as a consequence, they directly underpin the development of cardiometabolic complications [1].

Recent studies have highlighted extracellular vesicles (EVs), cell-derived membranous vesicles secreted in the extracellular environment, as relevant carriers of biological messages. Plasmatic EV levels [2–4] and EV markers [5] have been found to be significantly higher in obese patients. Moreover, WAT-derived EVs show

**CONTACT** Soazig Le Lay  [soazig.lelay@inserm.fr](mailto:soazig.lelay@inserm.fr)  INSERM UMR 1063 "Oxidative stress and metabolic pathologies", Institut de Biologie en Santé, 4 rue Larrey, Angers F-49933, France

\*These authors contributed equally to this work.

 Supplemental data for this article can be accessed [here](#).

© 2017 The Author(s). Published by Informa UK Limited, trading as Taylor & Francis Group.

This is an Open Access article distributed under the terms of the Creative Commons Attribution-NonCommercial License (<http://creativecommons.org/licenses/by-nc/4.0/>), which permits unrestricted non-commercial use, distribution, and reproduction in any medium, provided the original work is properly cited.

immunomodulatory properties in that they are able to convert macrophages towards a pro-inflammatory phenotype *in vitro* [6] and to modulate insulin signalling in muscle and liver cells [7]. Systemic injection of EVs from obese WAT explants into lean mice mediates the activation of macrophage-induced insulin resistance, highlighting their potential pathophysiological roles [8]. Many studies have confirmed the ability of different adipocyte models to secrete EVs, including rat isolated adipocytes [9,10], 3T3-L1 cell adipocytes [11] and a human preadipocyte differentiated cell model [6]. In addition, specific cellular stimuli enhance the secretion of adipokines, including adiponectin [12] and aP2/FABP4 [13,14], through their association with EVs. Moreover, adiponectin was detected in plasmatic EV samples [15], suggesting that adipocyte-derived EVs may be active vectors of communication *in vivo*.

Two types of EV can be generally distinguished [16]. Microvesicles are shed from the plasma membrane as a consequence of cytoskeleton reorganisation combined with negatively charged phosphatidylserine (PS) exposure in the outer membrane [17,18]. Exosomes are endosome-derived vesicles formed in multivesicular bodies (MVBs) and released after the fusion of these with the plasma membrane [16]. Besides their distinct intracellular origin, microvesicles and exosomes also represent two EV subtypes with different size ranges: microvesicles (50 nm/100 nm to 1  $\mu$ m) are described as being bigger than exosomes (30–100 nm). However, the terminology “exosomes” has been widely used for small EVs, regardless of their endolysosomal cellular origin, therefore denoting a mix of EVs from different intracellular origins and with distinct functional properties. Moreover, specific subsets of proteins, long considered to be exosomal markers, appear to be EV-enriched proteins since they may also be retrieved in other EV subtypes [19]. Considering the biological complexity of EVs, which is further influenced by the cellular context, no standardised analysis procedure has yet been validated to allow a clear separation of microvesicles from exosomes. Therefore, a combination of technical approaches appears to be essential to provide clues about the biological composition and functions of EV populations [20].

Despite the demonstrated ability of fat cells to secrete a considerable amount of EVs [21], adipocyte EV subtypes and their compositions have been poorly defined. The aim of this study was to quantitatively and qualitatively define fat cell-derived EV subpopulations through a combination of microscopic, biochemical and high-resolution mass-spectrometry (MS) technologies. By isolating adipocyte-derived EV subtypes through differential centrifugation steps, we demonstrated the secretion of two distinct populations,

termed small extracellular vesicles (sEVs) and large extracellular vesicles (lEVs). Based on our results, we show that these two EV subtypes can be distinguished based on specific protein and lipid signatures, and differential responses to stimuli. This work provides evidence that the different EV subtypes secreted by 3T3-L1 mature adipocytes display distinct biological and biochemical properties, and could predict different metabolic responses in recipient cells and/or tissues.

## Methods

### Reagents

All reagents, unless otherwise specified, were obtained from Sigma Aldrich (Saint-Quentin Fallavier, France).

Oleic acid (OA) and palmitic acid (PA) were conjugated to bovine serum albumin (BSA) as previously described, before their incubation in cell media [22]. Tumour necrosis factor- $\alpha$  (TNF $\alpha$ ) was obtained from Miltenyi Biotec (Paris, France) and interferon- $\gamma$  (INF $\gamma$ ) Immunotools (Friesoythe, Germany).

### Cell culture

3T3-L1 cells were maintained in high-glucose Dulbecco's modified Eagle's medium (DMEM) with 10% donor calf serum at 37°C and 10% carbon dioxide (CO<sub>2</sub>) as previously described [23]. In brief, 3T3-L1 cells were induced to differentiate 2 days post-confluence in DMEM 10% foetal bovine serum (FBS) by adding 250  $\mu$ M 3-isobutyl-1-methylxanthine (IBMX), 1.25  $\mu$ M dexamethasone (Dex) and 250 nM insulin for 3 days, and then cultured with 100 nM insulin alone until complete adipocyte differentiation (days 6–8). EVs were isolated from 24 h serum-free conditioned media of mature 3T3-L1 adipocytes (days 6–8 of differentiation) from at least four 15 cm diameter plates. Treatment of overnight serum-deprived mature adipocytes was performed for 24 h before EV isolation with the following agents: BSA-conjugated OA and PA (500  $\mu$ M), 8-bromoadenosine 3',5'-cyclic monophosphate (8-Br-cAMP) (1  $\mu$ M), ionomycin (1.5  $\mu$ M), angiotensin II (10 nM), TNF $\alpha$  (10 ng/mL) and INF (100U/mL corresponding to 5ng/mL).

### Isolation of primary adipocytes from murine adipose tissues

Adipocytes were isolated by collagenase digestion of 3–4 g of visceral fat pads from 4–6-month-old mice by the method of Rodbell [24] and cultured in endothelial cell growth medium supplemented with 4-(2-hydroxyethyl)-1-piperazineethanesulphonic acid

(HEPES) (10 mM) and albumin fatty acid free (0.1%), pH 7.4. EV subpopulations were isolated from 24 h serum-free conditioned media. The number of isolated adipocytes present in the fat-digested tissue was estimated by indirect calculation based on the mean cell volumes of fat cells (following measurements of fat cell diameters on microscopic images of isolated adipocyte suspensions), the lipid content of the dissected fat pads and lipid density (0.915) according to a well-described protocol [25].

### Production and isolation of EVs

Serum-free conditioned media were collected to isolate total EVs, IEVs and sEVs. The conditioned medium was first spun at  $1500 \times g$  for 20 min to remove cells and cell debris. Total EVs were pelleted by direct ultracentrifugation of the cell-cleared conditioned medium at  $100,000 \times g$  for 1 h at  $4^\circ\text{C}$  (rotor MLA-50, Beckman Coulter Optima MAX-XP Ultracentrifuge). After two washing steps in NaCl 0.9% (rotor TLA 100.4, Beckman Optima TLX Ultracentrifuge), total EV pellets were resuspended in NaCl. IEVs were recovered from cell-cleared supernatants following centrifugation at  $13,000 \times g$  for 60 min, followed by two washing steps in NaCl, and resuspended in sterile NaCl. sEVs were further isolated from IEV-depleted supernatants following a  $100,000 \times g$  ultracentrifugation step for 1 h at  $4^\circ\text{C}$  (rotor MLA-50, Beckman Coulter Optima MAX-XP Ultracentrifuge) and two washes in NaCl (see Figure 1(A)). The protein amount in the EV preparations was estimated by a DC protein assay (BioRad, Marnes la Coquette, France) using BSA as a standard.

### Separation of EVs on sucrose gradients

First, 500  $\mu\text{L}$  of IEVs or sEVs (corresponding to a total protein content of 120  $\mu\text{g}$ ) was loaded on top of a sucrose density gradient in an SW40 tube. The density gradient was prepared by layering successive sucrose solutions (31 fractions of 350  $\mu\text{L}$ ) of decreasing density (2.0 M to 0.4 M) on top of 700  $\mu\text{L}$  2.5 M sucrose, as previously described [26]. After ultracentrifugation at  $200,000 \times g$  for 18 h at  $4^\circ\text{C}$ , 12 fractions of 1 mL were collected. Fraction 1 (1 mL from the top of the gradient) was not further analysed, since proteins sticking to the tube wall were recovered in this fraction in an unspecific manner (data not shown). Sucrose density was measured on an aliquot of each fraction using a refractometer. Five millilitres of phosphate-buffered saline (PBS) was added to each 1 mL fraction collected, before recentrifugation at  $100,000 \times g$  for 70 min at  $4^\circ\text{C}$ . Pellets (visible or not) were resuspended in 50  $\mu\text{L}$

PBS, and divided into two aliquots of 25  $\mu\text{L}$  before storage at  $-80^\circ\text{C}$  and their further analysis by sodium dodecyl sulphate–polyacrylamide gel electrophoresis (SDS-PAGE).

### Cell lysates, SDS-PAGE and immunoblotting

Adipocytes were resuspended in lysis buffer [50 mM Tris pH 7.4, 0.27 M sucrose, 1 mM Na-orthovanadate pH 10, 1 mM ethylenediaminetetraacetic acid (EDTA), 1 mM ethylene glycol-bis( $\beta$ -aminoethyl ether)- $N,N,N',N'$ -tetraacetic acid (EGTA), 10 mM Na  $\beta$ -glycerophosphate, 50 mM NaF, 5 mM Na pyrophosphate, 1% (w/v) Triton X-100, 0.1% (v/v) 2-mercaptoethanol and cOmplete™ Protease Inhibitor Cocktail, (Roche Diagnostics, Meylan, France)]. Whole cell lysates were centrifuged at  $15,000 \times g$  for 10 min at  $4^\circ\text{C}$  and stored at  $-80^\circ\text{C}$ .

Cell lysates (8  $\mu\text{g}$ ), EV preparations (8  $\mu\text{g}$ ) and sucrose gradient-isolated fractions were diluted with Laemmli Buffer 6X (in reducing conditions, except for tetraspanin detection, where DTT was excluded), subjected to SDS-PAGE on 4–12% bis-acrylamide resolving gels (Novex® NuPAGE® precast gels; Life Technologies, Saint Aubin, France) and transferred on to nitrocellulose membranes (GE Healthcare, Pittsburgh, PA, USA). The membrane was blocked for 90 min at room temperature in 5% (w/v) BSA/Tris-buffered saline (TBS) (50 mM Tris-HCl pH 7.6, 150 mM NaCl) supplemented with 0.1% (v/v) Tween-20. Antibodies for Western blot were: adiponectin (PA1-054; Thermo Scientific, Villebon sur Yvette, France), actinin-4 (GTX15648; Genetex, Hsinchu, Taiwan), Alix (#611620; BD Biosciences, Le Pont de Claix, France), annexin A2 (#610068; BD Biosciences), aP2/FABP4 (#2120; Cell Signaling, ZA Leiden, The Netherlands),  $\beta$ -actin (#4970, clone 13E5; Cell Signaling), caveolin-1 (#SC-894, N20; Santa Cruz Biotechnology, Heidelberg, Germany), CD9 (#553758; BD Biosciences), CD63 (#D263-3, MBL International, Woburn, Massachusetts, USA), CD81 (#sc-18877; Santa Cruz Biotechnology), endoplasmic reticulum chaperone protein (ERp72) (#ADI-SPA-850; Enzo Life Sciences, Villeurbanne, France), fatty acid synthase (FAS) (a gift from Isabelle Dugail, INSERM, Paris, France), flotillin-2 (#610383; BD Biosciences), Mfge8 (#D199-3; MBL), major vault protein (MVP) (#ab2376; Abcam, Paris, France), Syntenin-1 (gift from Pascale Zimmerman, Centre de Recherche en Cancérologie de Marseille; or #ab19903, Abcam), TSG101 (GTX70255; Genetex), 14-3-3 (#8312; Cell Signaling, detect all isoforms). Nitrocellulose membranes were washed three times in TBS 0.1% Tween-20 (v/v) for 5 min before incubation with horseradish peroxidase (HRP)-coupled secondary antibodies (Jackson Immuno-Research, West Grove, Pennsylvania, USA). Protein signals were visualised using enhanced chemiluminescence (Immunocruz, Santa Cruz

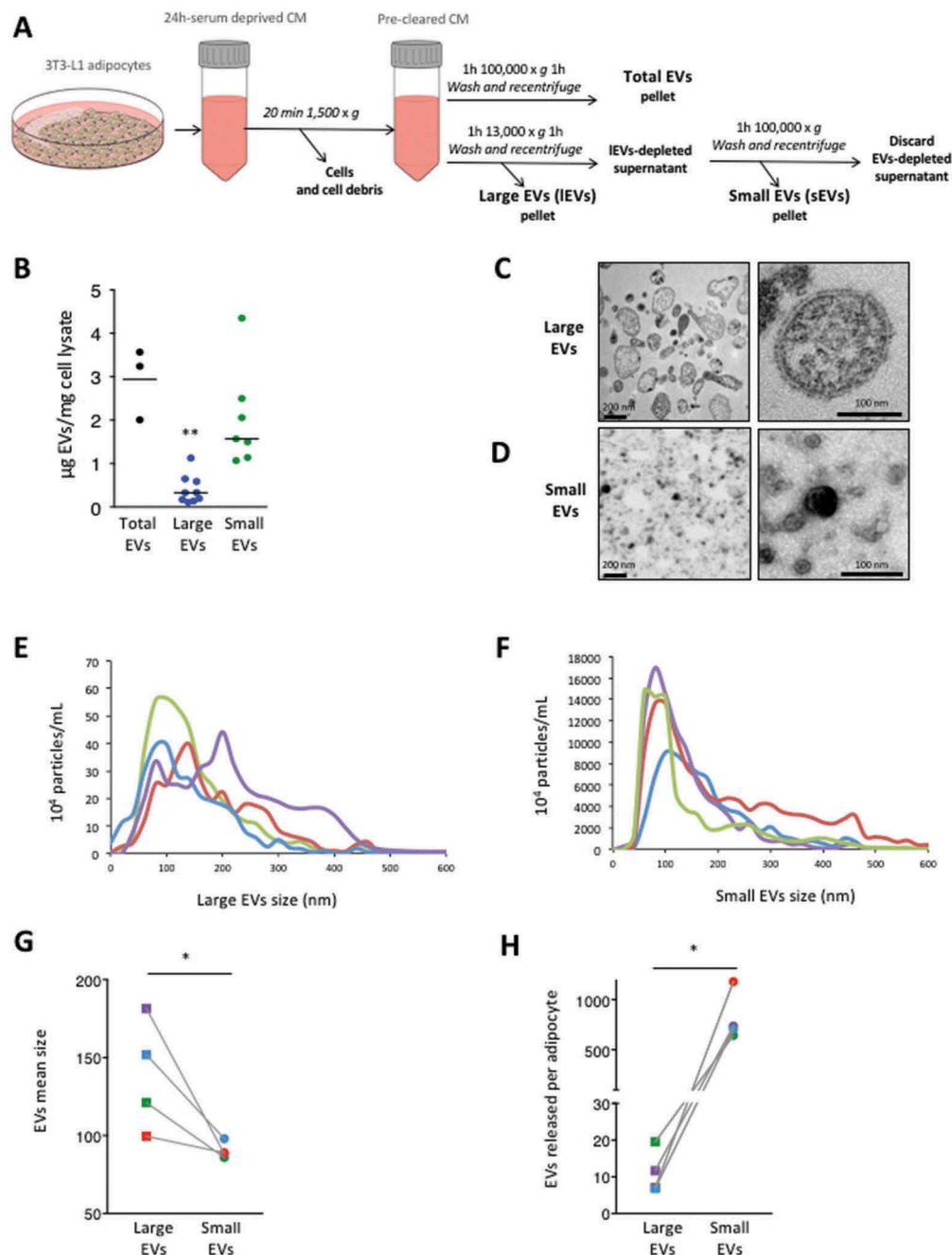


**Figure 1.** 3T3-L1 adipocytes secrete distinct extracellular vesicle (EV) subpopulations: large extracellular vesicles (IEVs) and small extracellular vesicles (sEVs). (A) Schematic representation of the successive differential centrifugation steps used to isolate the EV subpopulations released by mature 3T3-L1 adipocytes. Total EVs and EV subtypes, namely IEVs and sEVs, were isolated from 24 h serum-deprived 3T3-L1 culture media (CM) after the removal of cells and cell debris. (B) EV production based on protein content of EV subtypes. The protein content of each EV pellet normalised to the protein content of the original productive 3T3-L1 adipocytes is presented.  $n = 3-9$  independent EV preparations,  $**p < 0.01$  (Mann-Whitney rank test). (C,D) Transmission electron microscopy images of IEV (C) and sEV (D) pellets. Note that scale bars differ between images (left images, scale bars = 200 nm; right images, scale bars = 100 nm). (E-H) Nanoparticle tracking analysis of IEV and sEV populations. Determination of size distribution and concentration of IEV (E) and sEV (F) preparations. Indicated concentrations refer to the initial concentration of EVs in the conditioned media from which they were isolated and are expressed as  $10^4$  particles/mL. Each coloured line represents the mean of five videos acquired for a single biological sample. EV mean size (G) and EVs released per cell (H) are presented. The same colours as in (E) and (F) are used to distinguish the four different IEV/sEV preparations analysed. IEV pellets contained vesicles of larger size than sEV pellets. 3T3-L1 adipocytes secrete substantially more sEVs than IEVs in serum-deprived conditions.  $n = 4$  biological samples for IEVs and for sEVs,  $*p < 0.05$  (Mann-Whitney rank test).

Biotechnology) with a Chemi-smart 5000 imager system (Vilber-Lourmat, Marne La Vallée, France).

### Nanoparticle tracking analysis

EV samples were diluted in sterile NaCl 0.9% before nanoparticle tracking analysis (NTA). NTA was undertaken using the NanoSight NS300 (Malvern Instruments, Malvern, UK) equipped with a 405 nm laser. Ninety-second videos were recorded in five replicates per sample with optimised set parameters (the detection threshold was set to 7 and 5, respectively, for lEVs and sEVs). Temperature was automatically monitored and ranged from 20°C to 21°C. Videos were analysed when a sufficient number of valid trajectories was measured. Data capture and further analysis were performed using the NTA software version 3.1. At least three independent biological samples of each EV subtype were analysed, and the presented results correspond to the mean of the five videos taken for a given biological sample.

### Electron microscopy

EV preparations were first fixed for 16 h at 4°C with 2.5% glutaraldehyde (LFG Distribution, Lyon, France) in 0.1 M Sorensen buffer pH 7.4. lEV and sEV fractions were then deposited on Formvar®-coated copper grids and negatively stained with phosphotungstic acid 1% (w/v) for 30 s. Grids were rinsed briefly with milliQ water and left to air dry. Grids were then observed with a Jeol JEM 1400 microscope (Jeol, Croissy sur Seine, France) operated at 120 keV.

### Proteomic analysis of EV content by MS

#### Protein in-gel digestion

After silver staining following the method of Shevchenko et al. [27], protein bands were excised from one-dimensional SDS-PAGE. Each lane of short migration was cut and washed for 15 min with an acetonitrile/100 mM ammonium bicarbonate mixture (1:1). Digestion was performed in 50 mM ammonium bicarbonate pH 8.0 and the quantity of modified trypsin (Promega, sequencing grade) was 0.1 µg per sample. Digestion was achieved for 6 h at 37°C. The supernatant was conserved. Peptides were extracted by 5% formic acid in water/acetonitrile (v/v). Supernatant and extracted tryptic peptides were dried and resuspended in 50 µL of 0.1% (v/v) formic acid and 2% (v/v) acetonitrile.

### Nano-liquid chromatography–tandem mass spectrometry: proteomic analysis

A Q Exactive (Thermo Fisher Scientific) coupled to an Eksigent 2D nano LC (AB-Sciex, MA, USA) was used for the nano-liquid chromatography–tandem mass spectrometry (LC-MS/MS) analysis. Four microlitres of sample was injected on the nano LC-Ultra system chain. The sample was loaded at 7.5 µL/min on the precolumn cartridge (C18, 5 µm, 120 Å, 20 mm Nanoseparations) and desalted with 0.1% formic acid. Then, peptides were separated with a gradient of acetonitrile on the reverse-phase column C18 (stationary phase: C18 Biosphere, 3 µm; column: 75 µm i.d., 150 mm; Nanoseparations). Buffers were 0.1% formic acid in water (A) and 0.1% formic acid in acetonitrile (B). The peptide separation was achieved with a linear gradient from 5% to 35% B for 40 min at 300 nL/min<sup>-1</sup> (total gradient of 50 min). Eluted peptides were analysed online using a nanoelectrospray interface. Ionisation (1.8 kV ionisation potential) was performed with stainless steel emitters (30 µm i.d.; Thermo Electron). Capillary temperature was 250°C. Peptide ions were analysed using Xcalibur 3.0.63 (Tune version 2.3.0.1765) with the following data-dependent acquisition steps: (i) full MS scan [mass-to-charge ratio (*m/z*) 400 to 1400]; and (ii) MS/MS. Step 2 was repeated for the eight major ions detected in step 1. Dynamic exclusion was set to 40 s. The lock mass option “best” was chosen, MS resolution was 70,000 at *m/z* 400, auto gain control was 3e6 and maximum injection time was 250 ms. For MS2, the resolution was 17,500 at *m/z* 400, auto gain control was 5e4 with a maximum injection time of 120 ms, the isolation window was *m/z* = 3, the normalised collision energy was 27, the underfill ratio was 3%, the intensity threshold was 1.3e4 and the charge state was 2, 3.

#### Data processing and bioinformatics analysis

The *Mus musculus* database was downloaded from the UniProt KB database site ([www.uniprot.org](http://www.uniprot.org), January 2015, 24,721 protein entries). This database was merged and, in conjunction with reverse and contaminant databases, searched by X!Tandem (Sledge Hammer version 2013.09.01.1, <http://www.thegpm.org/tandem/>) using X!TandemPipeline (version 3.3.3) developed by the PAPPISO platform (<http://pappiso.inra.fr/bioinfo/>). Enzymatic cleavage was declared as a trypsin digestion with one possible miscleavage. Cys carboxyamidomethylation and Met oxidation were set to static and possible modifications, respectively. The precursor mass was 10 ppm and the fragment mass tolerance was 0.02 Da. A refinement search was added

with similar parameters except for semi-trypsinic peptide and possible N-ter proteins. For proteomic data, only peptides with an E value smaller than 0.1 were reported. Identified proteins were filtered and grouped using X!TandemPipeline (<http://pappso.inra.fr/bioinfo/xtandempipeline/>) according to the following requirements: (i) a minimum of two different peptides with an E value smaller than 0.0; and (ii) a protein log (E value, calculated as the product of unique peptide E values) smaller than  $2.10^{-3}$ . These criteria led to a peptide false discovery rate (FDR) of 0.27% when all conditions were combined. To take redundancy into account, proteins with at least one peptide in common were grouped. This allowed the grouping of proteins with similar functions. Within each group, proteins with at least one specific peptide relative to other members of the group were reported as subgroups. Only proteins detected on at least two biological replicates, based on their identification by at least two distinct peptides, were taken into account for qualitative analysis.

Label-free quantification of proteins was achieved using two different quantification methods: peptide quantification by spectral counting (SC) [28] and extracted ion chromatography (XIC) analysis [29]. The first method, SC, is based on the number of mass spectra (obtained with tryptic peptides in MS) assigned to one protein and is correlated with protein abundance. This quantification is based on the fact that the more of a particular protein is present in a sample, the more MS spectra are detected for peptides of that protein. This approach allows detection of the absence or presence of a given protein, but tends to overestimate the amount of low-abundance proteins because of the shared peptides with high-abundance proteins, resulting in low resolution to detect small abundance changes. In this analysis, a difference of five spectra between each EV subpopulation for a protein was set as the filter. The second method, XIC analysis, involves the quantification of the ion precursor (surface area) of a given peptide, the intensity of which is correlated with the protein abundance. The XIC-based approach has higher accuracy, sensitivity and specificity as it can detect low peptide quantities in a sample, but it cannot support qualitative variations in a given protein (presence/absence). MassChroQ software [30] was used for the XIC approach. All the previously identified peptides were selected for quantification. XIC extraction was performed using a peak detection threshold between 30,000 and 50,000 and a range of 10 ppm. XIC analyses were performed on  $\log_{10}$ -transformed data. Peptides showing a standard deviation of retention time higher than 40 s were removed. Peptides were quantified based on XIC using MassChroQR\_0.2.0.

### Experimental design and statistical rationale

Concerning the samples used for MS experiments, four independent biological replicates were generated for each of the three EV subpopulations studied (EVs, IEVs and sEVs). Using four replicates gave the best compromise to duly handle experimental variability and to perform quantitative analysis. All statistical procedures were carried out under the R v3.1.1 environment [31] using base packages developed by the PAPPISO platform (<http://pappso.inra.fr/index.php?>). Only peptides present in less than 2% of the sample and belonging to multiple proteins were removed. Changes in protein abundance were detected by analysis of variance. For both methods (XIC and SC), proteins were considered significant when the adjusted *p* value was  $< 0.05$ .

### Lipidomic analysis by MS

EV lipid content was extracted with the methyl-tert-butyl ether (MTBE) method according to Matyash et al. [32]. Lipid extracts were resuspended in 500  $\mu$ L  $\text{CHCl}_3/\text{MeOH}$  1:1, and 12:0/13:0 phosphatidylethanolamine (PE), 17:0/20:4 PE, 14:1/17:0 PE, 12:0/13:0 phosphatidylcholine (PC), 17:0/20:4 PC, 14:1/17:0 PC, 17:0 lysophosphatidylcholine (LPC), TG-Mix LM6000, sphingolipid (SP)-Mix LM6002 (2  $\mu$ M each) 12:0/13:0 PS, 17:0/20:4 PS, 14:1/17:0 PS, diacylglycerol (DG)-Mix LM6001 (3  $\mu$ M each), 12:0/13:0 phosphatidylinositol (PI), 17:0/20:4 PI and 14:1/17:0 PI (3.5  $\mu$ M each) were added as internal standards. Two microlitres were injected on a Thermo Hypersil GOLD C18,  $100 \times 1$  mm, 1.9  $\mu$ m high-performance liquid chromatography (HPLC) column, used with an Accela HPLC (Thermo Scientific). Solvent A was water with 1% ammonium acetate and 0.1% formic acid, and solvent B was acetonitrile/2-propanol 5:2 with 1% ammonium acetate and 0.1% formic acid. The gradient ran from 35% to 70% solvent B in 4 min, then to 100% solvent B in another 16 min, where it was held for 10 min. The flow rate was 250  $\mu$ L/min.

Data acquisition was basically performed according to Fauland et al. [33] by an Orbitrap-MS (LTQ-Orbitrap, Thermo Scientific) full scan in preview mode at a resolution of 100 k and  $< 2$  ppm mass accuracy with external calibration. The spray voltage was set to 5000 V, capillary voltage 35 V and the tube lens 120 V. Capillary temperature was 250°C. From the FT-MS preview scan, the 10 most abundant *m/z* values were picked in data-dependent acquisition mode, fragmented in the linear ion trap analyser and ejected at nominal mass resolution. Normalised collision energy was set to 35%, the repeat count was 2 and the

exclusion duration was 1 min. Data were further analysed using Lipid Data Analyzer, a custom-developed software tool described in more detail by Hartler et al. [34].

### Cholesterol measurement

Cholesterol content was measured on isoproterenol-resuspended EV preparations using a commercial kit (Thermo Scientific). The absorbance of the cholesterol-based reaction was measured at 510 nm, and cholesterol concentration was calculated based on a cholesterol standard curve also made using isoproterenol.

### Annexin V binding analysis

Annexin V binding properties to both adipocyte-derived IEVs and sEVs were measured by flow cytometry using the kit Annexin V-FITC (Miltenyi Biotec). Five microlitres of IEVs (corresponding to 0.5 µg of IEV content) were washed with annexin V 1X binding buffer, centrifuged at  $13,000 \times g$  for 15 min, then incubated with 5 µL of annexin V-FITC in annexin V 1X buffer in the dark for 45 min. Following staining, IEVs were washed twice in annexin V 1X buffer, pelleted and resuspended in 200 µL of annexin V 1X buffer for flow cytometry analysis. Given the small size of exosomes, 5 µg of sEVs was combined with 10 µL latex beads (Molecular Probes A37304) as described previously [35]. sEV-coated beads were labelled with annexin V-FITC (or annexin V 1X buffer as a background control) for 45 min in the dark, and washed with annexin V 1X buffer. Annexin V positivity was determined on a MACSQuant flow cytometer. Data were further analysed using MACSQuant analysis software.

### Statistical analysis

Statistical analysis of the results was performed using non-parametric tests such as the Mann–Whitney or Wilcoxon signed-rank test, respectively, for comparison of non-paired or paired samples. The differences were considered significant for  $p$  values  $< 0.05$  and stated as follows: \* for  $p < 0.05$ , \*\* $p < 0.01$  and \*\*\* $p < 0.001$ .

## Results

### 3T3-L1 adipocytes secrete two EV size populations: IEVs and sEVs

EVs were isolated from 24 h serum-free conditioned media of 3T3-L1 mature adipocytes using ultracentrifugation-based isolation (Figure 1(A)). Considering the limited contribution of apoptosis to adipose tissue

development and the fact that 3T3-L1 preadipocytes acquire a relative resistance to apoptosis as they differentiate, we did not investigate the secretion of apoptotic bodies from adipocytes.

Absolute quantification, based on EV protein content, reveals that the sEV population was predominant over IEVs (Figure 1(B)). Transmission electron microscope (TEM) imaging of EV preparations allowed further visualisation of the morphological characteristics of these two EV subpopulations. The IEV fraction included a heterogeneous population of vesicles, with a well-delimited double membrane, differing greatly in size, shape and electron density (Figure 1(C)). Conversely, the sEV fraction corresponded to a pool of smaller spherical vesicles of similar sizes, with cup-shaped morphology (Figure 1(D)). Size distribution analysis of both EV subtypes, based on diameter measurements of both EV subpopulations on TEM images, indeed showed distinct size patterns for IEVs and sEVs (Figure S1). NTA confirmed different size distributions between the two EV preparations, with a higher dispersion in large vesicles for IEV preparations (Figure 1(E)), whereas sEVs peaked between 80 and 120 nm (Figure 1(F)). Therefore, these two subpopulations of EVs differ greatly in size, as illustrated by a mean size ranging between 100 and 200 nm for IEVs, and close to or below 100 nm for sEVs (Figure 1(G)). Furthermore, IEV concentrations were several hundred times lower than sEV concentrations, confirming the ability of 3T3-L1 adipocytes to secrete sEVs in large proportions (Figure 1(E,F)). Once normalised per emitting cell, a mature 3T3-L1 adipocyte will secrete an average of  $11 \pm 5$  IEVs and  $843 \pm 185$  sEVs (Figure 1(H)).

### Adipocyte-derived IEVs and sEVs both express classical EV markers but display different flotation behaviours on sucrose gradients

A few proteins are widely used to characterise exosomes, and more largely mixed EV populations, including Alix, tetraspanins and lipid-raft associated proteins such as caveolins and flotillins [20,36]. We thus compared the association of these EV markers by analysing on Western blots the same amount of proteins from each EV isolated pellet (total EVs, IEVs and sEVs) or from the secreting adipocyte cell lysates (Figure 2(A)). As expected, total EVs secreted by 3T3-L1 adipocytes harbour tetraspanins (CD9, CD63, CD81), Alix and Mfge8, as well as caveolin-1 and flotillin-2 (Figure 2(A)). Separation between IEV and sEV subpopulations revealed that the membranous lipid-raft proteins caveolin-1 and flotillin-2 were preferentially associated with the IEV fraction (Figure 2(A,B)). The same was true for Mfge8,



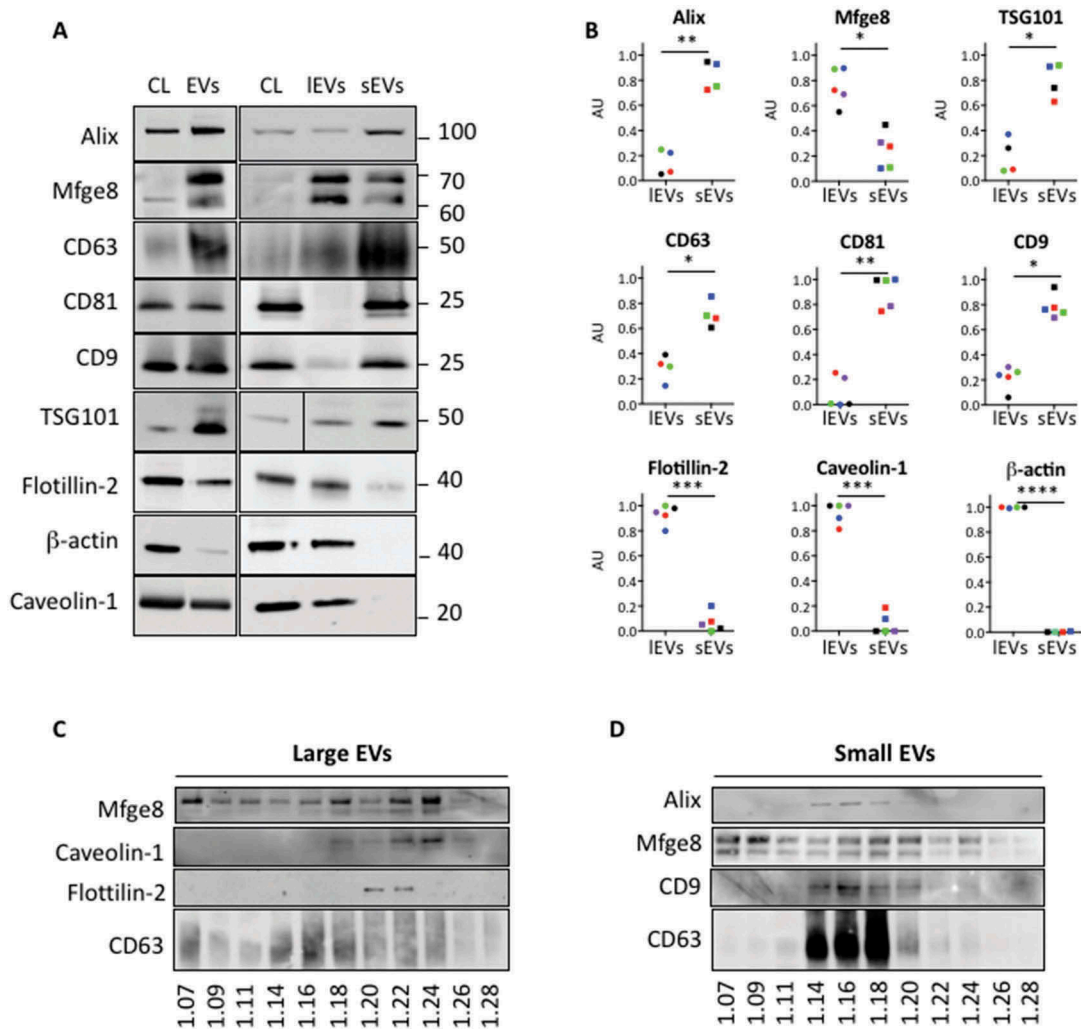


**Figure 2.** Adipocyte-derived large extracellular vesicles (IEVs) and small extracellular vesicles (sEVs) differentially carry classical extracellular vesicle (EV) markers and display different flotation behaviours on sucrose gradients. (A) Western blot analysis of different EV markers in EV subpopulations isolated from adipocytes. The different centrifugation pellets, including either total EVs or IEVs and sEVs, were resuspended in NaCl and quantified for their protein content. IEVs ( $13,000 \times g$  pellet) and sEVs ( $100,000 \times g$  pellet) were collected from the same batch of cells cultured in the same conditions (see Methods). Eight micrograms of total adipocyte-derived EVs (EVs), IEVs or sEVs was loaded on a sodium dodecyl sulphate–polyacrylamide gel electrophoresis (SDS-PAGE) gel, together with  $8 \mu\text{g}$  of original adipocyte cell lysate (CL), and analysed by immunoblotting for the presence of the following proteins: Alix, Mfge8, the tetraspanins CD63, CD81 and CD9, TSG101, flotillin-2,  $\beta$ -actin and caveolin-1. Ten micrograms of EVs and CL were specifically loaded to allow detection of  $\beta$ -actin in the total EV sample. One representative blot for each protein is presented. (B) Quantification of the distribution of the different EV markers between IEVs and sEVs, analysed by Western blot. At least three independent preparations of IEVs and sEVs were analysed for the presence of the EV markers by Western blot, following equal protein loading ( $8 \mu\text{g}$ ). For each protein analysed, the signal intensity (SI) of the protein signal band was calculated using ImageJ software, as follows:  $AU_{IEVs} = (SI_{IEVs}) / (SI_{IEVs} + SI_{sEVs})$  and  $AU_{sEVs} = (SI_{sEVs}) / (SI_{IEVs} + SI_{sEVs})$ . Each colour represents an independent experiment, with IEV and sEV preparations derived from the same secreting cells. \* $p < 0.05$  (paired Student's  $t$  test), \*\* $p < 0.01$ , \*\*\*\* $p < 0.0001$ . (C,D) Separation of IEV (C) and sEV (D) preparations on sucrose gradients. Equivalent protein amounts of IEVs and sEVs ( $120 \mu\text{g}$ ) resuspended in  $500 \mu\text{L}$  NaCl were loaded on to a sucrose gradient (2.0 M to 0.4 M). Collected sucrose fractions were recentrifuged, resuspended in phosphate-buffered saline and divided into two portions, to be loaded on SDS-PAGE in either reducing or non-reducing conditions, the latter gel being used for tetraspanin detection. The density of the collected sucrose fractions was determined by a refractometer and is indicated above the gel. IEV- and sEV-derived sucrose density fractions were probed with the following EV markers: Alix, Mfge8, CD63, CD9 and  $\beta$ -actin. IEV pellets were found to float mainly at densities between 1.20 and 1.22 g/mL, according to Mfge8, caveolin-1, flotillin-2 and CD63 signals (C). Alix was undetectable in this IEV-separated sucrose gradient. By contrast, sEV pellets were recovered at lower densities, between 1.14 and 1.20 g/mL, as illustrated by Alix, Mfge8, CD63 and CD9 signals (D).

consistent with the relative abundance of this peripheral membrane protein in IEVs [19].  $\beta$ -Actin was exclusively recovered in the IEV fraction, and undetectable in the sEV fraction (data not shown), in agreement with the critical role of cytoskeleton remodelling in the process of microvesicle shedding [37]. By contrast, sEVs were significantly enriched with Alix, the endosomal sorting complexes required for transport I (ESCRT-I) component TSG101 and the tetraspanins CD9, CD63 and CD81 (Figure 2(A,B)).

Since differential ultracentrifugation protocols allow recovery of a crude pellet of the EV population, a classic way to improve the separation of membrane-enclosed vesicles is to allow the EV pellet to float into an overlying sucrose gradient. The distribution of EV markers is then studied in the collected fractions following IEV and sEV sucrose density gradient separation. By this means, we observed that IEVs were mainly recovered in density fractions between 1.20 and 1.22 g/mL, according to caveolin-1 and flotillin-2 signals (Figure 2(C)). The sEVs floated at lighter densities, between 1.14 and 1.20 g/mL, as illustrated by CD9, CD63 and Alix detection (Figure 2(D)), in agreement with densities and markers generally described in the literature [16]. Mfge8 presented a large pattern of expression over the IEV and sEV-derived fractions (Figure 2(C,D)). By contrast, Alix was undetectable in IEV-derived sucrose fractions (data not shown) and CD63 was only weakly expressed (Figure 2(C)). Taken together, these results show different biochemical properties for IEV and sEV subpopulations associated with differential expression of classical EV markers and distinct sucrose flotation properties.

### **Adipocyte-derived IEVs and sEVs exhibit a specific protein signature**

To further characterise the protein composition of adipocyte EV subpopulations, we performed label-free quantitative proteomic analysis from four biological replicates of total EVs, IEV and sEV populations using MS. We identified 533 proteins, corresponding to 408 groups of proteins (0.268% FDR peptides) from all EV subgroups (Dataset S1).

This qualitative analysis allowed the identification of 217, 480 and 168 proteins in total EV, IEV and sEV fractions, respectively (Dataset S2). A more conservative filtering was applied to consider proteins present in EV fractions based on the detection of at least two distinct peptides in two different biological replicates (see the Methods section). A list of the identified proteins, categorised according to gene ontology (GO) annotations in the UniProt KB database, is presented in Dataset S3. This included EV protein markers such

as tetraspanin CD81, the associated ESCRT-complex protein Alix and the glycoprotein Mfge8. Defence and immunity proteins, including class I major histocompatibility complex molecules and immunoglobulins, were also detected, as expected [38]. In addition, multiple proteins known to be involved in membrane trafficking, such as Rab proteins, annexins, small guanosine triphosphate (GTP)-binding proteins and several cytoskeletal-related proteins (e.g. actin, tubulin,  $\alpha$ -actinin and myosin), were identified. Numerous proteins with enzymatic activities or enzyme modulators, mainly derived from mitochondria, were also present, thus illustrating the trapping of the cytosolic part during EV biogenesis. Furthermore, nucleic acid binding proteins such as histones and ribosomal proteins were found in the different EV subclasses. The presence of extracellular matrix (ECM) proteins additionally illustrates the membranous origin of EVs. The identification of signalling molecules such as complement factors, lipoprotein lipase and the adipocyte-secreted hormone adiponectin indicated the potential role of adipocyte-derived EVs in systemic haemostasis and/or glucidolipidic metabolism. Finally, the presence of many transporters, transfer and carrier proteins, receptors and signalling proteins highlights the ability of such EVs to bind and/or transfer information to recipient cells, therefore modulating their metabolism and/or phenotype.

Comparison of the protein composition between the different EV fractions showed that sEVs quasi-overlap total EV protein content (Figure 3(A)). Conversely, the IEV fraction, which represented the most enriched fraction in terms of protein diversity, had 31.5% and 24.6% of proteins in common with total EVs and sEVs, respectively (Figure 3(A)). Furthermore, principal component analysis (PCA) of these qualitative comparisons highlighted the distinct protein composition of the IEV fraction, compared to sEVs and total EVs (Figure 3(B)). The co-segregation of total EVs and sEVs (Figure 3(B)) is probably due to the higher proportion of sEVs secreted by adipocytes, in comparison to adipocyte-secreted IEVs (see Figure 1(B)). To explore whether these different protein compositions may reflect different functional properties of EV subclasses, we performed a GO term enrichment classification of proteins for IEV and sEV fractions. Based on a GO cellular component analysis, we highlighted a specific enrichment of IEVs in membrane, organelles and cell part components in comparison with sEVs, in agreement with membrane-derived shedding of microvesicles (Figure 3(C)). In contrast, the sEV fraction was specifically enriched in ECM and macromolecular complex components (Figure 3(C)). Subsequent

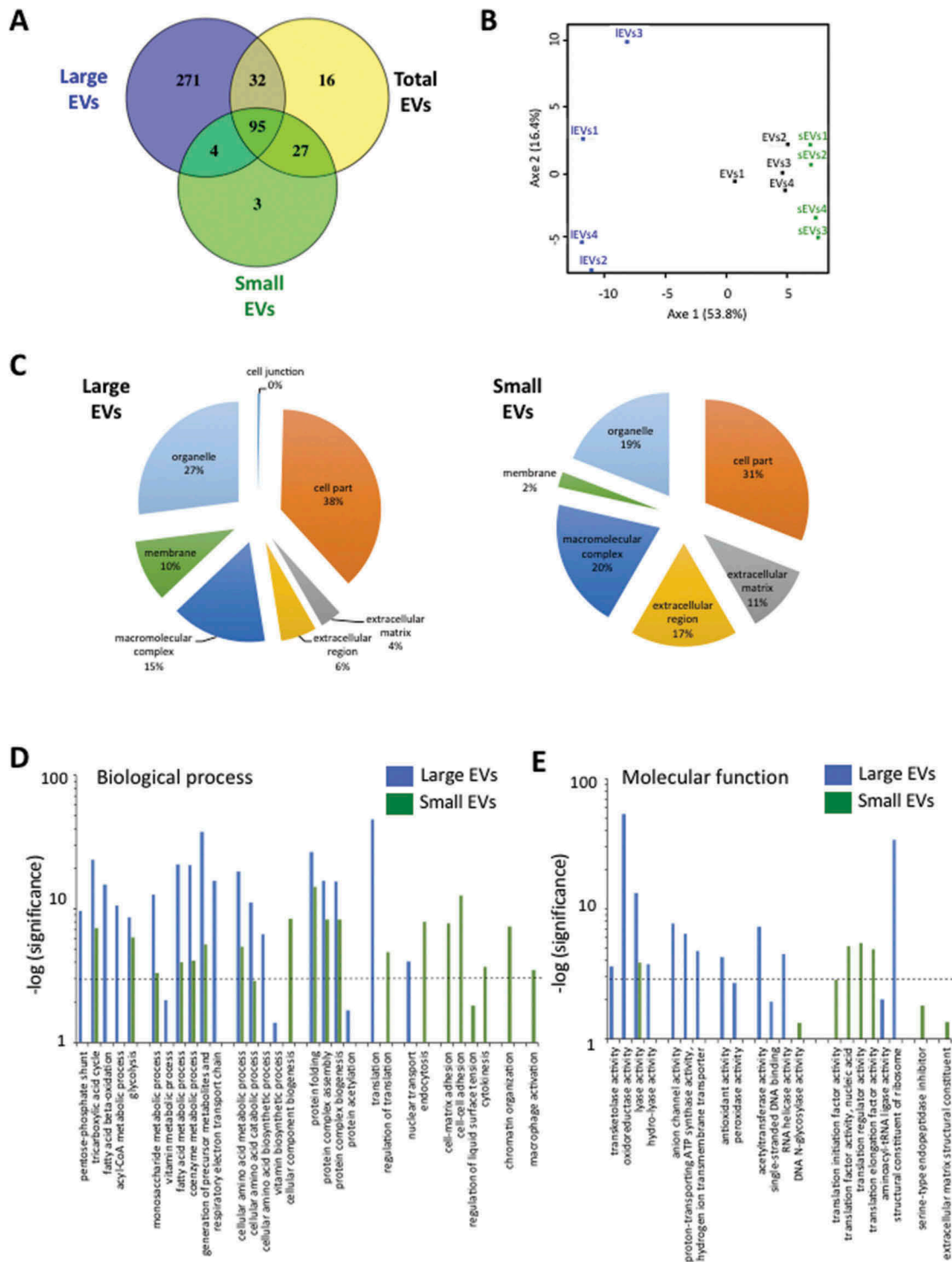


**Figure 3.** Proteome characterisation by nano-liquid chromatography–tandem mass spectrometry (LC-MS/MS) analysis reveals the specific protein signature of extracellular vesicle (EV) subpopulations. (A) Venn diagram of the identified proteins in total EV, large extracellular vesicle (IEV) and small extracellular vesicle (sEV) populations. Proteins were considered identified when at least two peptides were detected in at least two of the four biological replicates. The important overlap between total EV and sEV proteomes underlines the ability of 3T3-L1 adipocytes to secrete abundant sEVs, in comparison to IEVs, in serum-deprived culture conditions. (B) Principal component analysis (PCA) of EV subpopulations underlines the distinct protein composition between sEV and IEV fractions. Results are shown for the four independent adipocyte-derived EV biological preparations (total EVs, IEVs and sEVs) analysed by nano-LC-MS/MS analysis. PCA of identified proteins for each EV subtype shows a clear separation of IEVs from sEVs and total EVs. (C–E) Gene ontology (GO) terms of protein families enriched in IEV and sEV preparations. Identified proteins in IEV and sEV fractions, respectively, were classified according to cellular component (C), biological process (D) and molecular function (E) categories defined by the GO consortium using the Panther classification system database. (C) Cellular component GO analysis reveals an enrichment of membrane and organelle components for IEVs, and in the extracellular region and extracellular matrix for sEV. (D,E) GO categories with greater than five-fold enrichment are presented for IEV and sEV populations following classification according to biological process (D) or molecular function (E). The  $[-\log(P)]$  is shown for each category indicated, where  $P$  is the significance. The dotted line represents the threshold ( $P = 0.01$ ) over which the represented categories display a significant five-fold greater enrichment than expected by chance.

analyses based on biological process GO enrichment identified the presence of proteins involved in many metabolic pathways for both IEVs and sEVs, most of them linked to mitochondrial function (Figure 3(D)). GO analysis for molecular function confirmed the presence of many mitochondrial enzymes in the IEV fraction, with a particular enrichment in oxydoreductases (Figure 3(E)). In addition, proteins falling in the categories “protein folding, complex assembly and biogenesis” (Figure 3(D)), as well as components such as enzymes and factors critical for translation pathways (Figure 3(E)), were overrepresented in both EV subpopulations. The sEV fraction revealed a specific enrichment in processes related to cell adhesion as well as in macrophage activation (Figure 3(D)). Altogether, proteomic analysis of adipocyte-secreted EV subpopulations demonstrates specific protein composition, which could predict different systemic metabolic responses.

### **Identification and validation of specific protein markers of adipocyte-derived IEVs and sEVs**

To identify and validate specific EV markers of IEV- and sEV-derived adipocytes, we performed a quantitative analysis of our proteomic data based on SC and XIC analysis of selected peptide ions (see Methods), two methods of analysis that have been shown to correlate well with protein abundances in complex biological samples [39,40]. Based on SC and XIC statistical analysis of the results ( $p < 0.05$ ), we were able to identify proteins that display significant enrichment in the IEV (Table 1) and sEV (Table 2) fractions.

Proteins that were specifically enriched in the IEV fractions were more abundant than in sEVs; this is likely to be related to the higher diversity of proteins recovered in the IEV fractions (Dataset S2). Among the classical class of protein families associated with EVs, we highlighted a specific enrichment of the IEV subpopulation in numerous metabolic enzymes, nucleic acid binding proteins (especially 40S and 60S ribosomal proteins), chaperones, including some heat shock proteins (HSP7 C, HSP90 $\beta$ , GRP78 and GRP75), cytoskeleton-related proteins (including actins and  $\beta$ -tubulin chains), membrane traffic proteins such as annexins and Rab GTPases, transporters (ADP/ATP translocase, mitochondrial channels, ATP synthase subunits and the fatty acid binding protein transporter FABP4/aP2) (Table 1). By contrast, sEV fractions were specifically enriched in ECM proteins, T-complex protein 1 chaperones, histones and MVP, as well as some metabolic enzymes involved in lipid and carbohydrate synthesis (Table 2). To validate the

statistical analysis of our quantitative proteomic data and to confirm the respective enrichment of proteins in the IEV and sEV subpopulations, we analysed the expression of a selection of proteins, highly expressed in adipocytes, by Western blot from equal loading of IEVs and sEVs on SDS-PAGE gels (Figure 4). This confirmed the specific enrichment of FABP4/aP2, 14-3-3, annexin A2 and endoplasmic reticulum chaperones in IEV preparations (Figure 4(A)), whereas MVP, FAS and adiponectin were specifically targeted to the sEV fraction (Figure 4(B)). We also investigated the enrichment of actinin-4 and syntenin-1, two proteins found in our proteomic analysis and recently described as potential novel markers of IEVs and sEVs, respectively [41,42]. Whereas we confirmed the specific association of actinin-4 with IEVs, syntenin-1 expression was equally detected in IEV and sEV preparations (Figure 4(C)).

Altogether, our analysis of adipocyte-derived EV proteomics data allowed us to identify EV markers for the IEV and sEV subpopulations, which could be further used to differentiate these two EV subtypes. Moreover, these markers formally identify EVs as potential cargos for the sorting and secretion of key adipocyte signalling proteins, such as adiponectin and FABP4/aP2, which are known to play critical roles in glucidolipidic metabolism at the level of the organism.

### **Adipocyte-derived IEVs and sEVs present specific lipid characteristics**

Besides protein-specific targeting to EVs, which may affect the signalling responses in recipient cells, lipids may also play critical roles in EV functions. To analyse in depth the lipid content of EV subpopulations, we performed a quantitative analysis of neutral lipids and phospholipids (PLs) by MS of IEV and sEV fractions, based on three independent biological samples for each subclass. Lipid concentrations (measured as  $\mu\text{g lipids}/\mu\text{g protein}$ ) in IEVs and sEVs showed that PLs and SPs constituted the main lipid classes retrieved from these EV preparations, whereas only traces of glycerolipids (GLs) were detected (Figure 5(A)). The molecular lipid species measured belonged to nine lipid classes, with five different types of PL (LPC, PC, PE, PI and PS); SPs, including ceramides (Cer), glycosylceramides (GlyCer) and sphingomyelin (SM); and diacylglycerols (DGs) representing the GLs (Figure 5(B)). PC represents by far the main PL (nearly 60% of total PL) present in IEVs and sEVs, whereas LPC, PS, PI and PE are proportionally minor PLs. SM is also particularly enriched in EV fractions and constitutes the main SP (23–24%) in adipocyte-derived EVs. Only small amounts of Cer (< 1%) and

**Table 1.** Proteins specifically enriched in large extracellular vesicle (IEV) preparations.

Protein class	Acc. no.	Entry name	Protein description	XIC		SC	
				IEV/sEV ratio	Quantification (p value)	Median of SC values (IEV/sEV)	Quantification (p value)
<b>Chaperones</b>							
	P08113	ENPL	Endoplasmic	2.2	2.0E-02	7/0.5	1.9E-02
	P11499	HS90B	Heat shock protein HSP 90-beta	1.7	3.6E-02	12/3	2.0E-02
	P20029	GRP78	78 kDa glucose-regulated protein	3.7	2.4E-04	13.5/1	1.8E-02
	<b>P38647</b>	<b>GRP75</b>	<b>Stress-70 protein, mitochondrial</b>	<b>3.0</b>	<b>2.8E-02</b>	<b>9/0</b>	<b>1.4E-02</b>
	P63017	HSP7 C	Heat shock cognate 71 kDa protein	NA	7.4E-01	10/2	2.0E-02
	<b>P63038</b>	<b>CH60</b>	<b>60 kDa heat shock protein, mitochondrial</b>	<b>3.7</b>	<b>4.1E-02</b>	<b>10/0</b>	<b>1.4E-02</b>
	<b>P63101</b>	<b>1433Z</b>	<b>14-3-3 protein zeta/delta</b>	<b>9.2</b>	<b>3.0E-06</b>	<b>4/0</b>	<b>NA</b>
	<b>Q9CQV8</b>	<b>1433B</b>	<b>14-3-3 protein beta/alpha</b>	<b>1.7</b>	<b>5.0E-02</b>	<b>4,5/0</b>	<b>NA</b>
<b>Cytoskeleton-related proteins</b>							
	<b>P13020</b>	<b>GELS</b>	<b>Gelsolin</b>	<b>4.1</b>	<b>3.9E-03</b>	<b>9.5/0</b>	<b>1.8E-02</b>
	<b>P26041</b>	<b>MOES</b>	<b>Moesin</b>	<b>6.3</b>	<b>2.5E-03</b>	<b>3.5/0</b>	<b>NA</b>
	P60710	ACTB	Actin, cytoplasmic 1	NA	NA	16/6	2.0E-02
	P63260	ACTG	Actin, cytoplasmic 2	NA	NA	15.5/6	2.0E-02
	P68368	TBA4A	Tubulin alpha-4A chain	1.9	1.6E-02	9.5/4.5	NA
	P68372	TBB4B	Tubulin beta-4B chain	NA	9.8E-01	10/2	2.8E-02
	P99024	TBB5	Tubulin beta-5 chain	NA	2.4E-01	10.5/3	2.0E-02
	<b>Q61879</b>	<b>MYH10</b>	<b>Myosin-10</b>	<b>1.5</b>	<b>1.4E-02</b>	<b>5.5/0</b>	<b>1.2E-01</b>
	Q8VDD5	MYH9	Myosin-9	NA	5.7E-02	7.5/2.5	2.1E-02
	Q9WTI7	MYO1 C	Unconventional myosin-1c	2.1	7.2E-03	11/0	1.7E-02
<b>Enzyme modulators</b>							
	P08752	GNAI2	Guanine nucleotide-binding protein G	12.2	1.6E-05	3.5/0	NA
	<b>P62880</b>	<b>GBB2</b>	<b>Guanine nucleotide-binding protein G</b>	<b>3.3</b>	<b>6.5E-04</b>	<b>4.5/0</b>	<b>NA</b>
<b>Membrane traffic proteins</b>							
	P07356	ANXA2	Annexin A2	3.0	7.1E-05	18/2	1.7E-02
	<b>P10107</b>	<b>ANXA1</b>	<b>Annexin A1</b>	<b>6.9</b>	<b>5.4E-06</b>	<b>9.5/0</b>	<b>1.4E-02</b>
	P14824	ANXA6	Annexin A6	2.1	5.1E-04	15/2.5	1.9E-02
	P48036	ANXA5	Annexin A5	3.9	3.6E-04	7.5/0	1.9E-02
	<b>P51150</b>	<b>RAB7A</b>	<b>Ras-related protein Rab-7a</b>	<b>2.8</b>	<b>9.6E-03</b>	<b>4/0</b>	<b>NA</b>
	P97429	ANXA4	Annexin A4	4.9	5.4E-04	7.5/0	1.7E-02
<b>Nucleic acid binding proteins</b>							
	P10126	EF1A1	Elongation factor 1-alpha 1	4.3	1.2E-04	6.5/1.5	2.1E-02
	<b>P25444</b>	<b>RS2</b>	<b>40S ribosomal protein S2</b>	<b>4.8</b>	<b>2.1E-03</b>	<b>2.5/0</b>	<b>NA</b>
	<b>P27659</b>	<b>RL3</b>	<b>60S ribosomal protein L3</b>	<b>4.2</b>	<b>1.9E-04</b>	<b>3.5/0</b>	<b>NA</b>
	<b>P47911</b>	<b>RL6</b>	<b>60S ribosomal protein L6</b>	<b>2.4</b>	<b>2.9E-02</b>	<b>4/0</b>	<b>NA</b>
	P62242	RS8	40S ribosomal protein S8	2.5	4.4E-02	4.5/1.5	NA
	<b>P62754</b>	<b>RS6</b>	<b>40S ribosomal protein S6</b>	<b>3.2</b>	<b>5.4E-03</b>	<b>5/0</b>	<b>NA</b>
	<b>P97351</b>	<b>RS3A</b>	<b>40S ribosomal protein S3a</b>	<b>2.4</b>	<b>2.2E-03</b>	<b>4/0</b>	<b>NA</b>
<b>Protein with enzymatic activities</b>							
	<b>O88844</b>	<b>IDHC</b>	<b>Isocitrate dehydrogenase [NADP] cytoplasmic</b>	<b>2.7</b>	<b>3.4E-04</b>	<b>4/0</b>	<b>NA</b>
	<b>P05064</b>	<b>ALDOA</b>	<b>Fructose-bisphosphate aldolase A</b>	<b>9.1</b>	<b>8.9E-06</b>	<b>6/0</b>	<b>1.7E-02</b>
	<b>P06151</b>	<b>LDHA</b>	<b>L-lactate dehydrogenase A chain</b>	<b>3.0</b>	<b>1.3E-02</b>	<b>3.5/0</b>	<b>NA</b>
	<b>P08249</b>	<b>MDHM</b>	<b>Malate dehydrogenase, mitochondrial</b>	<b>NA</b>	<b>1.4E-01</b>	<b>9.5/0</b>	<b>1.4E-02</b>
	<b>P10852</b>	<b>4F2</b>	<b>4F2 cell-surface antigen heavy chain</b>	<b>22.0</b>	<b>1.4E-04</b>	<b>6.5/0</b>	<b>NA</b>
	<b>P14152</b>	<b>MDHC</b>	<b>Malate dehydrogenase, cytoplasmic</b>	<b>5.0</b>	<b>8.4E-04</b>	<b>3.5/0</b>	<b>NA</b>
	P17182	ENOA	Alpha-enolase	2.2	2.2E-03	7.5/1.5	2.1E-02
	P17751	TPIS	Triosephosphate isomerase	3.5	1.7E-04	4.5/1	NA
	<b>P24270</b>	<b>CATA</b>	<b>Catalase</b>	<b>4.7</b>	<b>2.4E-04</b>	<b>6.5/0</b>	<b>1.3E-02</b>
	<b>P35700</b>	<b>PRDX1</b>	<b>Peroxiredoxin-1</b>	<b>7.0</b>	<b>4.6E-04</b>	<b>4/0</b>	<b>NA</b>
	P41216	ACSL1	Long-chain fatty-acid-CoA ligase 1	NA	5.4E-01	24/8	2.0E-02
	<b>P51660</b>	<b>DHB4</b>	<b>Peroxisomal multifunctional enzyme type 2</b>	<b>2.9</b>	<b>9.7E-03</b>	<b>4.5/0</b>	<b>1.4E-02</b>
	<b>Q00519</b>	<b>XDH</b>	<b>Xanthine dehydrogenase/oxidase</b>	<b>8.9</b>	<b>2.0E-02</b>	<b>2/0</b>	<b>NA</b>
	<b>Q8BMS1</b>	<b>ECHA</b>	<b>Trifunctional enzyme subunit alpha, mitochondrial</b>	<b>NA</b>	<b>2.4E-01</b>	<b>9/0</b>	<b>1.4E-02</b>
	Q9EQ20	MMSA	Methylmalonate-semialdehyde dehydrogenase [acylating], mitochondrial	2.8	2.6E-02	4.5/0.5	NA
	<b>Q921H8</b>	<b>THIKA</b>	<b>3-Ketoacyl-CoA thiolase A, peroxisomal</b>	<b>1.3</b>	<b>3.8E-02</b>	<b>1/0</b>	<b>NA</b>
	<b>Q99LC5</b>	<b>ETFA</b>	<b>Electron transfer flavoprotein subunit alpha, mitochondrial</b>	<b>3.5</b>	<b>1.6E-03</b>	<b>4.5/0</b>	<b>NA</b>
<b>Transporter, transfer and carrier proteins</b>							
	P04117	FABP4	Fatty acid-binding protein, adipocyte	3.3	2.6E-03	9/0.5	1.9E-02
	<b>P48962</b>	<b>ADT1</b>	<b>ADP/ATP translocase 1</b>	<b>NA</b>	<b>2.0E-01</b>	<b>5/0</b>	<b>1.3E-02</b>
	<b>P51881</b>	<b>ADT2</b>	<b>ADP/ATP translocase 2</b>	<b>6.5</b>	<b>1.5E-02</b>	<b>5.5/0</b>	<b>1.4E-02</b>
	P56480	ATPB	ATP synthase subunit beta, mitochondrial	NA	5.4E-01	13/4	2.0E-02
	Q03265	ATPA	ATP synthase subunit alpha, mitochondrial	6.3	5.2E-03	9/1	1.7E-02
	<b>Q8VDN2</b>	<b>AT1A1</b>	<b>Sodium/potassium-transporting ATPase subunit alpha-1</b>	<b>7.3</b>	<b>7.7E-04</b>	<b>5/0</b>	<b>NA</b>

(Continued)

Table 1. (Continued).

Protein class	Acc. no.	Entry name	Protein description	XIC		SC	
				IEV/sEV ratio	Quantification ( <i>p</i> value)	Median of SC values (IEV/sEV)	Quantification ( <i>p</i> value)
<b>Miscellaneous</b>							
	<b>O35129</b>	<b>PHB2</b>	<b>Prohibitin-2</b>	<b>NA</b>	<b>5.2E-02</b>	<b>7/0</b>	<b>1.4E-02</b>
	<b>P09103</b>	<b>PDIA1</b>	<b>Protein disulphide-isomerase</b>	<b>5.6</b>	<b>7.0E-05</b>	<b>4.5/0</b>	<b>NA</b>
	<b>P27773</b>	<b>PDIA3</b>	<b>Protein disulphide-isomerase A3</b>	<b>3.1</b>	<b>8.8E-05</b>	<b>9/0</b>	<b>1.1E-02</b>
	<b>P67778</b>	<b>PHB</b>	<b>Prohibitin</b>	<b>7.3</b>	<b>7.4E-03</b>	<b>6/0</b>	<b>4.7E-02</b>
	<b>Q922R8</b>	<b>PDIA6</b>	<b>Protein disulphide-isomerase A6</b>	<b>1.9</b>	<b>4.2E-02</b>	<b>3/0</b>	<b>NA</b>

Protein enrichment in large extracellular vesicle (IEV) and small extracellular vesicle (sEV) subpopulations was compared, and significant statistical enrichment of proteins in IEVs, based on spectral counting (SC) and extracted ion chromatography (XIC) analysis, is presented. Enrichment was considered on the basis of a difference of at least five spectra between at least two biological samples. The *p* values and ratio calculated following SC and XIC analysis are presented. The XIC ratio was calculated with the median of area peptides (for one protein) from the four independent replicates of IEVs divided by the median of all peptides (for the same protein) from the four independent replicates of sEVs. The SC ratio corresponds to the median of SC detected for one protein in the four independent replicates of IEVs to the median of SC detected for the same protein in the four independent replicates of sEVs. Proteins were considered enriched in IEVs when *p* < 0.05 following XIC and/or SC analysis. Proteins exclusively found in IEV samples are shown in bold. Those *p* values not found to be statistically different are in grey. Acc. no., accession number; NA, not available.

GlyCer (< 1%) were measured. Finally, DGs, at 1%, illustrated the trace amount of GLs. Absolute molar concentrations of these different lipid classes were unchanged between total EVs, IEVs and sEVs, confirming a similar PL and neutral lipid profile for these different EV subpopulations (Figure S2). Closer examination of the molecular profile of the fatty acid composition of EV-associated lipids did not reveal significant changes, either in acyl chains lengths or in the degree of fatty acid saturation for PLs (Figure S3), SPs and GLs (Figure S4).

This lipidomic analysis was completed by total cholesterol measurement based on a colorimetric assay. Whereas PL are by far the main constituent of cell membranes, membrane cholesterol content is a key determinant of membrane structure and dynamics. We measured significantly higher cholesterol content in sEVs than in IEVs (relative to total EV protein content) (Figure 5(C)), therefore identifying this high sterol content as a characteristic trait of adipocyte sEV populations.

Since microvesicle shedding is known to happen following the loss of membrane asymmetry, leading to the subsequent exposure of PS [17], we also sought to investigate PS exposure in EV subpopulations, by measuring their annexin V positivity by flow cytometry. Despite the absence of quantitative changes in PS content between IEVs and sEVs (see Figure S2), we highlighted that 60% of PS associated with the IEV fractions was externalised, whereas the sEV fractions showed very low annexin V positivity (Figure 5(D)). Thus, sEV and IEV populations could be distinguished on the basis of their cholesterol content and externalised PS.

These results therefore identify new lipid markers that may affect the biological responses to EVs in recipient cells.

### Secretion of IEVs and sEVs from adipocytes is induced by stimuli related to the chronic low-grade inflammation state of obesity

We next investigated whether the secretion of adipocyte-derived EVs may be enhanced by external stimuli in the context of the chronic low-grade inflammation state associated with obesity. For this purpose, we selected stimuli that are known to be relevant in the context of adipose tissue hypertrophy [43–45] and have also been identified as enhancing EV secretion. Therefore, IEV and sEV subpopulations were collected after 24 h exposure to calcium ionophore ionomycin [46,47], PA, OA [12,22], 8-Br-cAMP mimicking prolonged lipolytic stimulation [14], angiotensin-II [48] and inflammatory cytokines such as TNF $\alpha$  and INF $\gamma$  [49,50]. These experiments were conducted in serum-free conditions and EV release was quantified by NTA (Figure 6(A)). First, we confirmed that ionomycin induced IEV secretion, in agreement with the well-established role of increased intracellular calcium in the shedding of plasma membrane-derived vesicles [46]. Moreover, we revealed the specific potency of PA, unlike OA, to significantly enhance secretion of both IEVs and sEVs (Figure 6(A,B)). Finally, our results also highlighted the induction of both IEV and sEV production following exposure to TNF $\alpha$ , whereas EV secretion was maintained at basal levels following INF $\gamma$  treatment (Figure 6B). No induction of EV secretion was observed following angiotensin II treatment.

Taken together, these data demonstrate the ability of specific stimuli, which have been described to take part in the metabolic complications associated with obesity, to stimulate IEV and/or sEV populations. Therefore, adipocyte-derived IEVs and sEVs may be viewed as messengers or relayers of metabolic responses associated with the pathophysiological context of obesity.

**Table 2.** Proteins specifically enriched in small extracellular vesicle (sEV) preparations.

Protein class	Acc. no.	Entry name	Protein description	XIC		SC	
				sEV/IEV ratio	Quantification ( <i>p</i> value)	Median of SC values (sEV/IEV)	Quantification ( <i>p</i> value)
<b>Chaperones</b>							
	P80314	TCPB	T-complex protein 1 subunit beta	2.9	1.6E-02	3.5/2	NA
	P80317	TCPZ	T-complex protein 1 subunit zeta	6.6	1.1E-02	0.5/2	NA
<b>Enzyme modulators</b>							
	P68040	GBLP	Guanine nucleotide-binding protein subunit beta-2-like 1	2.5	8.9E-03	3.5/6.5	NA
<b>Extracellular matrix proteins</b>							
	P02468	LAMC1	Laminin subunit gamma-1	7.9	1.1E-03	4.5/1	NA
	P10493	NID1	Nidogen-1	7.7	1.9E-03	9.5/2	5.8E-02
	<b>P11087</b>	<b>CO1A1</b>	<b>Collagen alpha-1</b>	<b>16.5</b>	<b>1.7E-04</b>	<b>4.5/0</b>	<b>NA</b>
	P11276	FINC	Fibronectin	36.8	3.4E-04	32.5/0	1.8E-02
	P37889	FBLN2	Fibulin-2	12.8	6.1E-06	24/2.5	2.1E-02
	P97927	LAMA4	Laminin subunit alpha-4	3.6	3.0E-03	6.5/2	NA
	Q02788	CO6A2	Collagen alpha-2	82.4	4.1E-06	32.5/0	1.8E-02
	Q04857	CO6A1	Collagen alpha-1	114.3	3.3E-06	42.5/4	2.1E-02
	Q07797	LG3BP	Galectin-3-binding protein	127.3	5.1E-06	23/0	1.8E-02
	<b>Q8CG85</b>	<b>MAMC2</b>	<b>MAM domain-containing protein 2</b>	<b>20.0</b>	<b>3.1E-04</b>	<b>5/0</b>	<b>1.4E-02</b>
	Q99K41	EMIL1	EMILIN-1	14.1	8.0E-05	13.5/0	1.7E-02
	<b>Q9VWJ9</b>	<b>FBLN4</b>	<b>EGF-containing fibulin-like extracellular matrix protein 2</b>	<b>6.5</b>	<b>3.8E-03</b>	<b>6/0</b>	<b>1.4E-02</b>
<b>Membrane traffic proteins</b>							
	Q9JHU4	DYHC1	Cytoplasmic dynein 1 heavy chain 1	2.3	1.1E-03	3.5/4.5	NA
	Q68FD5	CLH1	Clathrin heavy chain 1	4.2	6.5E-04	24.5/17	3.9E-01
<b>Nucleic acid binding proteins</b>							
	P10853	H2B1F	Histone H2B type 1-F/J/L	5.6	3.0E-02	6.5/3.5	NA
	P62806	H4	Histone H4	4.5	2.5E-02	13.5/9.5	NA
	P14206	RSSA	40S ribosomal protein SA	1.8	3.6E-02	3.5/3.5	NA
	Q9EQK5	MVP	Major vault protein	35.1	4.1E-08	30.5/2.5	1.9E-02
<b>Proteins with enzymatic activities</b>							
	P12382	PFKAL	ATP-dependent 6-phosphofructokinase, liver type	2.2	1.7E-02	0.5/2.5	NA
	P19096	FAS	Fatty acid synthase	3.3	3.2E-03	28/20	6.6E-01
	P28271	ACOC	Cytoplasmic aconitate hydratase	2.7	3.5E-04	3.0/3.0	NA
	P54310	LIPS	Hormone-sensitive lipase	2.5	3.5E-04	3.0/4	NA
	P97873	LOXL1	Lysyl oxidase homologue 1	5.2	3.3E-02	6.5/3.5	NA
	Q00612	G6PD1	Glucose-6-phosphate 1-dehydrogenase X	8.8	1.5E-02	0/2	NA
	Q01853	TERA	Transitional endoplasmic reticulum ATPase	3.1	7.8E-04	3.5/3.5	NA
	Q5SWU9	ACACA	Acetyl-CoA carboxylase 1	13.4	1.3E-04	15.0/1	2.8E-02
<b>Signalling molecules</b>							
	P11152	LIPL	Lipoprotein lipase	4.2	1.6E-03	13.5/8.5	NA
	Q60994	ADIPO	Adiponectin	8.8	8.5E-04	4.5/1.5	NA
<b>Miscellaneous</b>							
	<b>P08003</b>	<b>Pdia4</b>	<b>Protein disulphide-isomerase A4</b>	<b>14.5</b>	<b>4.5E-05</b>	<b>0/1.5</b>	<b>NA</b>

Protein enrichment in large extracellular vesicle (IEV) and small extracellular vesicle (sEV) subpopulations was compared and significant enrichment of proteins in sEVs, based on spectral counting (SC) and extracted ion chromatography (XIC) analysis, is presented. Enrichment was considered on the basis of a difference of at least five spectra between at least two biological samples. The *p* values and ratio calculated following SC and XIC analysis are presented. The XIC ratio was calculated with the median of area peptides (for one protein) from the four independent replicates of sEVs divided by the median of area peptides (for the same protein) from the four independent replicates of IEVs. The SC ratio corresponds to the median of SC detected for one protein in the four independent replicates of sEVs to the median of SC detected for the same protein in the four independent replicates of IEVs. Proteins were considered enriched in sEVs when *p* < 0.05 following XIC and/or SC analysis. Proteins exclusively found in sEV samples are shown in bold. Those *p* values not found to be statistically different are in grey. Acc. no., accession number; NA, not available.

### **Murine primary adipocytes secrete IEVs and sEVs with similar morphological and biochemical characteristics to EVs secreted by 3T3-L1 adipocytes**

We next investigated whether such EV secretion also happens *in vivo*. We therefore studied EV release by isolating adipocytes from murine visceral fat pads, cultured for 24 h in serum-free conditions. EV isolation of cell-cleared conditioned media revealed the ability of primary adipocytes to secrete both IEVs and sEVs in similar proportions, based on EV protein content secreted per gram of dissected

adipose tissue (Figure 7(A)). Electron microscopy imaging (Figure 7(B)) and NTA (Figure 7(D)) confirmed the presence of IEVs and sEVs in the pelleted material at 13,000 × *g* and 100,000 × *g*, respectively. Isolated EV subpopulations from primary adipocytes presented similar morphological traits and sizes (Figure 7(E)) to 3T3-L1 adipocyte-derived EVs (Figure 1). NTA corroborates the equal secretion of IEVs and sEVs by isolated adipocytes, corresponding to 82.4 ± 12.8 IEVs and 101.8 ± 66.9 sEVs secreted per isolated adipocyte, in contrast to 3T3-L1, which secreted mainly sEVs. Finally, biochemical analysis of these EV subpopulations confirms the specific

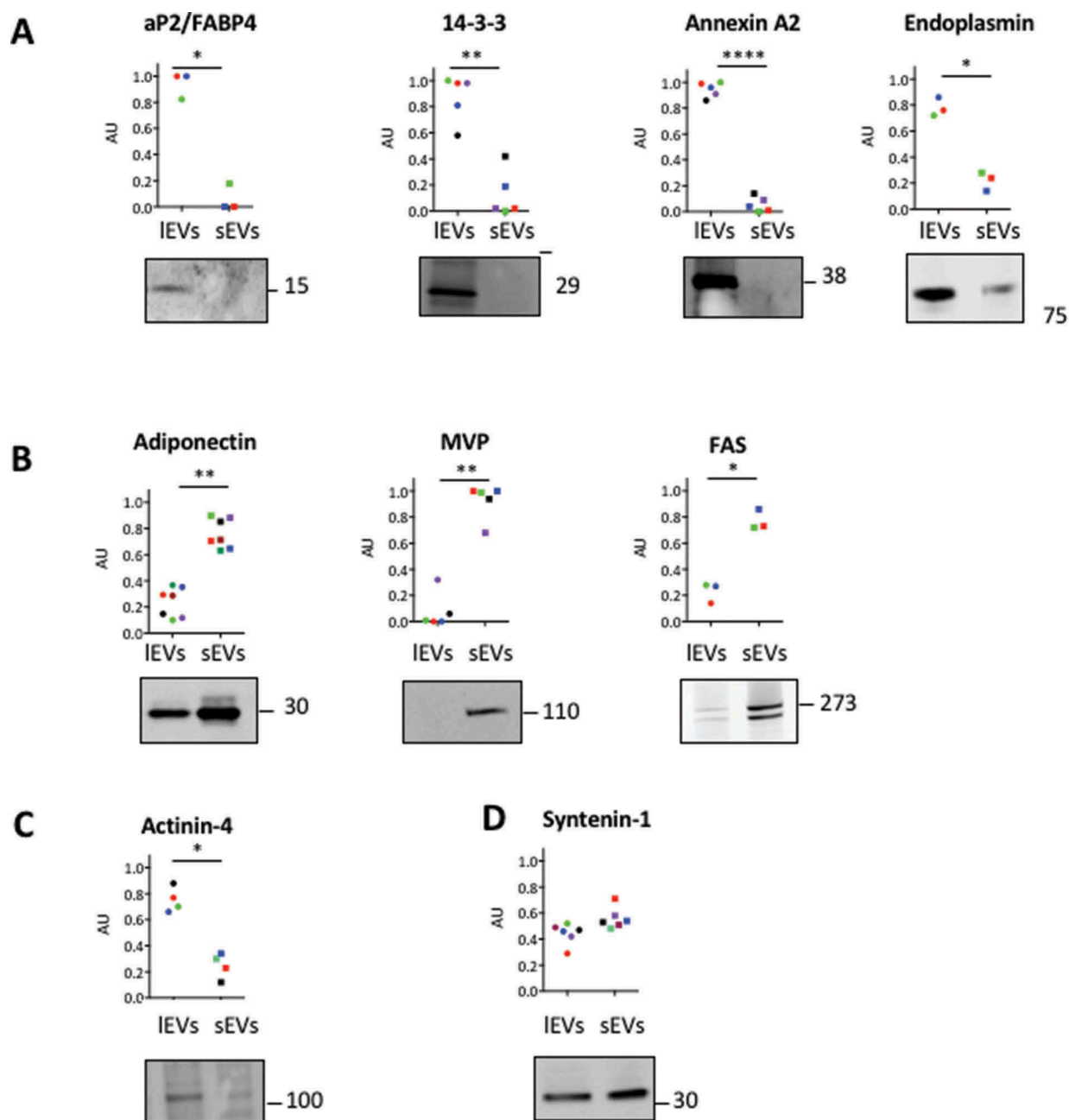


**Figure 4.** Validation of proteomics data and identification of specific markers of large extracellular vesicles (IEVs) and small extracellular vesicle (sEVs). (A,B) Western blot analysis of selected proteins identified by the quantitative analysis of proteomic data. Equal amounts of protein (8  $\mu$ g) for IEVs or sEVs were loaded on a sodium dodecyl sulphate–polyacrylamide gel electrophoresis gel and immunoblotted for selected proteins found to be enriched in either IEV or sEV preparations, based on the statistical analysis of quantitative proteomic data. For each selected protein, a representative immunoblot is presented. Quantifications of signal intensity are represented as dot plots and calculated from three to seven independent experiments as described in Figure 2 (B). The colours used represent different biological replicates used for the immunoblots. These results were confirmed by immunoblotting the specific enrichment of ap2/FABP4, 14-3-3, annexin A2 and endoplasmin in IEV fractions, whereas adiponectin, major vault protein (MVP) and FAS are specifically enriched in sEV fractions. (C,D) Western blot of actinin-4 (C) and syntenin-1 (D) in IEV and sEV subpopulations. Actinin-4 is found to preferentially associate with IEVs, whereas syntenin-1 expression is equally distributed in IEV and sEV preparations.

association of the tetraspanins CD9 and CD63 with sEVs, whereas the membranous proteins flotillin-2 and caveolin-1 were preferentially retrieved in IEVs.

These results highlight the ability of *in vivo* adipocytes to secrete non-negligible amounts of EVs, which can be separated into small and large subpopulations. The IEVs



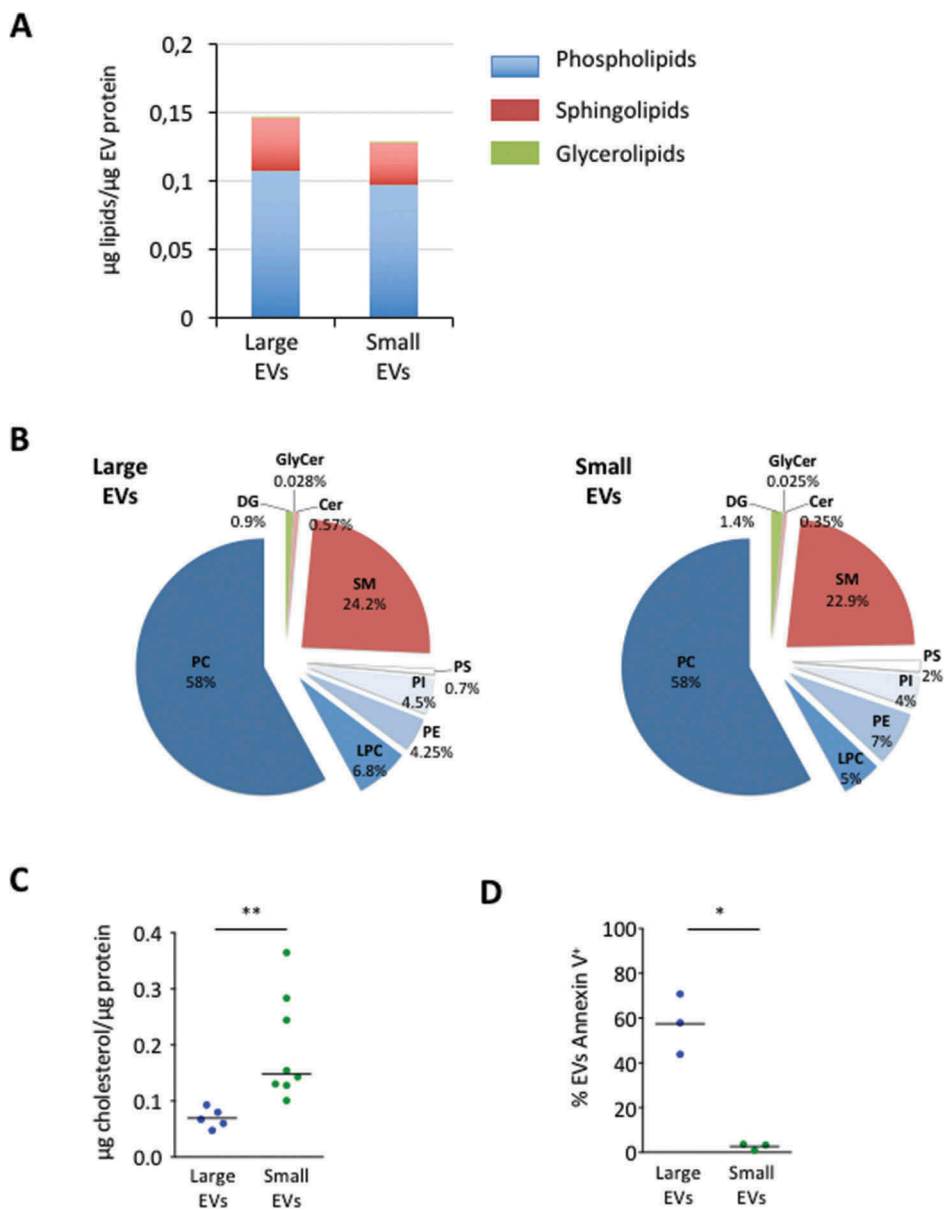


**Figure 5.** Lipidomic characterisation of large extracellular vesicles (IEVs) and small extracellular vesicles (sEVs) by liquid chromatography–tandem mass spectrometry (LC-MS/MS). (A) The total amount of IEV and sEV membrane lipids as determined by LC-MS/MS is expressed in micrograms normalised to the amount of extracellular vesicle (EV) protein content. The term phospholipids represents the sum of phosphatidylcholine (PC), phosphatidylethanolamine (PE), phosphatidylinositol (PI) and phosphatidylserine (PS). Sphingolipids include ceramides (Cer), glycosylceramides (GlyCer) and sphingomyelin (SM). Glycerolipids are uniquely represented by diacylglycerols (DGs). Data presented for each lipid concentration represent the mean of four individual IEV and sEV preparations each. (B) Composition of IEV and sEV membrane lipids according to lipid classes. Data are expressed as a percentage of the total lipid content determined for each statistical group and represent the mean of four individual IEV and sEV preparations each. See (A) for definitions of each lipid species. (C) sEV preparations are specifically enriched in cholesterol. The cholesterol content was measured in isopropanol-resuspended EV membrane lipids using a colorimetric assay. The total amount of cholesterol measured is expressed in micrograms normalised to the amount of EV protein content.  $n = 5–8$  biological samples for IEVs and for sEVs,  $*p < 0.05$  (Mann–Whitney rank test). (D) Measurement of annexin V positivity of adipocyte-derived IEVs and sEVs by flow cytometry. High annexin V binding of adipocyte-derived IEVs illustrates a higher proportion of externalised PS in IEVs than in sEV preparations.  $n = 3$  independent IEV and sEV preparations,  $*p < 0.05$  (paired Student's *t* test)

and sEVs had physical and biological characteristics similar to those described for 3T3-L1, predicting differential functional effects on target cells and/or tissues.

## Discussion

Emerging roles of EVs in the pathophysiology of many diseases have revealed technical pitfalls and potential

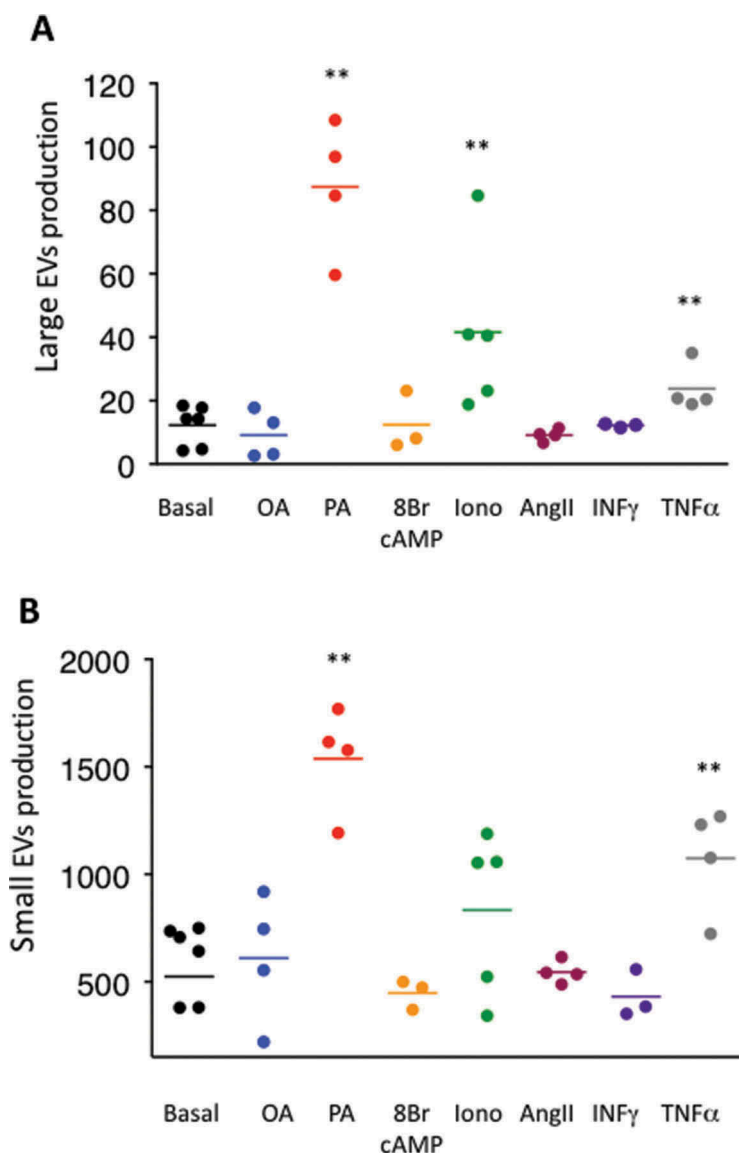


**Figure 6.** Large extracellular vesicle (IEV) and small extracellular vesicle (sEV) secretion following exposure to external stimuli. (A,B) Nanoparticle tracking analysis quantification of IEV (A) and sEV (B) secretion following 24 h treatment of 3T3-L1 mature adipocytes in serum-deprived conditions with the following stimuli: bovine serum albumin-conjugated oleic or palmitic acid (OA or PA, 500  $\mu$ M each), 8-bromo-adenosine 3',5'-cyclic monophosphate (8-Br-cAMP) (1  $\mu$ M), ionomycin (Iono, 1.5  $\mu$ M), angiotensin II (AngII, 10 nM), interferon- $\gamma$  (INF $\gamma$ , 100 U/mL corresponding to 5 ng/mL) and tumour necrosis factor- $\alpha$  (TNF $\alpha$ , 10 ng/mL). Extracellular vesicles secreted per adipocyte are represented as dot plots and calculated from three to five independent experiments. \* $p < 0.05$ , \*\* $p < 0.01$  (Mann-Whitney rank test).

artefacts, which need to be addressed to fully clarify the properties of EVs and their biological significance [20]. In addition, the heterogeneity between EV subclasses pinpoints the need to identify and define EV subtypes before characterising their functional properties [41,42].

The present study aimed to present a comprehensive overview of EV subtypes secreted by 3T3-L1 mature adipocytes by separating IEV populations (probably including microvesicles) from sEV subsets (including exosomes). We provide evidence that IEVs and sEVs present distinct biological and biochemical properties based on: (i) distinct

morphological and size parameters; (ii) different sucrose flotation properties; (iii) distinct protein patterns; (iv) subtle changes in their lipid content and distribution; and (v) specific responses to biological stimuli.

Our data confirm that adipocytes secrete significant amounts of EVs, including IEVs and sEVs. By comparison to the secretion of exosomes measured previously [11,21], we obtained a similar amount of sEVs, highlighting adipocytes as a provider of sEVs, which could be assimilated to exosomes as previously described in adipocytes. Indeed, the secretion of adipocyte-derived exosomes has been

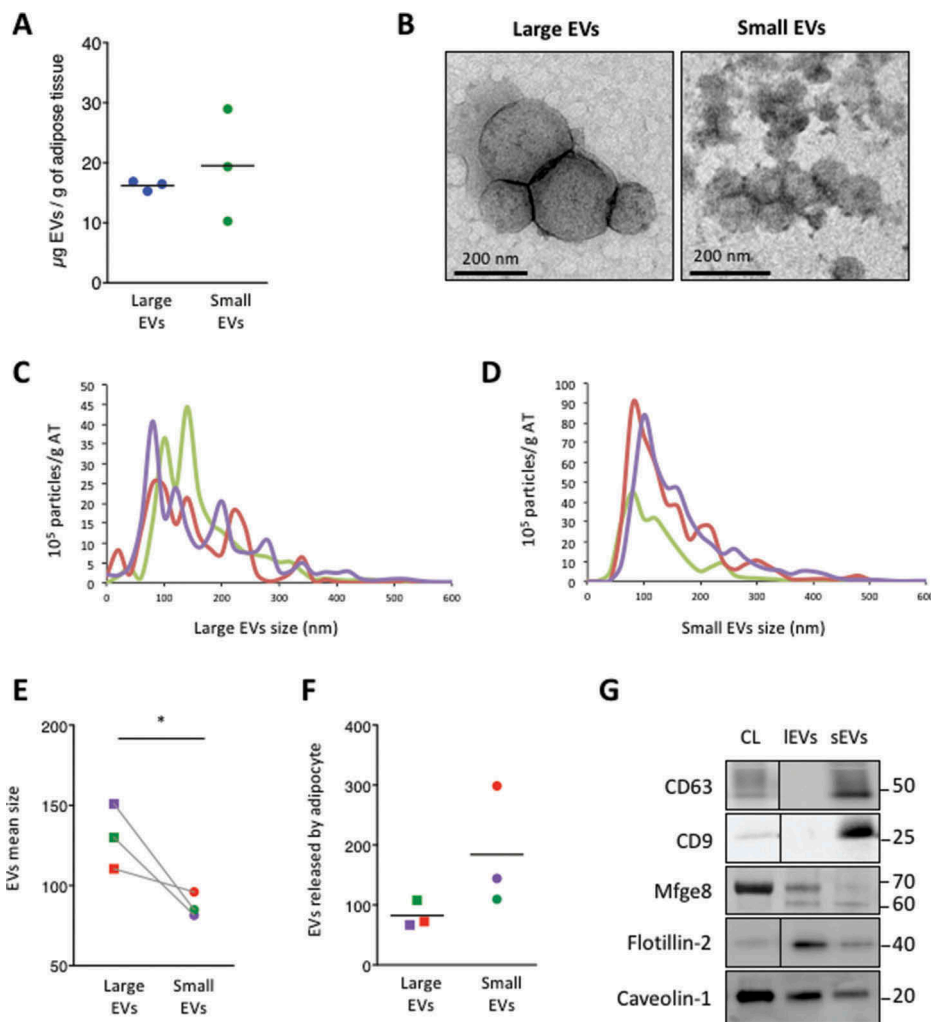


**Figure 7.** Primary adipocytes secrete large extracellular vesicles (IEVs) and small extracellular vesicles (sEVs), compared to 3T3-L1 adipocytes. (A) Primary adipocyte-derived extracellular vesicle (EV) production based on protein content of EV subtypes. The protein content of each EV pellet per gram of dissected adipose tissue is presented. Similar production of IEVs and sEVs was measured.  $n = 3$  independent EV preparations. (B) Transmission electron microscopy images of IEV and sEV pellets. Scale bars = 200 nm. (C–F) Nanoparticle tracking analysis of IEV and sEV populations. Determination of size distribution and concentration of IEV (C) and sEV (D) preparations. Indicated concentrations refer to the concentration of EVs secreted per gram of dissected adipose tissue and are expressed as  $10^5$  particles/g adipose tissue. Each coloured line represents the mean of five videos acquired for a single biological sample. EV mean size (E) and EVs released per cell (H) are presented. The number of isolated adipocytes from dissected fat pads was indirectly estimated, as described in the Methods section. The same colours are used in C–F to distinguish the three different IEV/sEV preparations analysed. IEV pellets contained larger vesicles than sEV pellets. Primary adipocytes secrete equal amounts of sEVs and IEVs when cultured in serum-deprived conditions.  $n = 3$  biological samples for IEVs and for sEVs,  $*p < 0.05$  (Mann–Whitney rank test). (G) Western blot analysis of different EV markers in EV subpopulations isolated from primary adipocytes: 8  $\mu\text{g}$  of either IEVs or sEVs was loaded on a sodium dodecyl sulphate–polyacrylamide gel electrophoresis gel, together with 8  $\mu\text{g}$  of original adipocyte cell lysate (CL), and analysed by immunoblotting for the presence of the following proteins: CD9, CD63, Mfge8, flotillin-2 and caveolin-1. A black line was inserted on the immunoblots when samples were loaded on the same gel, but not side by side. One representative blot for each protein is presented.

estimated to be 10-fold higher than exosome secretion from cancerous melanoma cell lines [21]. Compared with this important sEV secretion by 3T3-L1 mature cells, IEV secretion appears to be negligible (around 100-fold lower than sEV secretion). Serum-deprived conditions, which are used to avoid contamination with serum-derived

exosomes, may, however, favour the secretion of basal exosomes and therefore contribute to the high proportion of secreted sEVs. Indeed, IEVs and sEVs were secreted in equivalent amounts from adipocytes isolated from visceral adipose tissue, reinforcing the need to distinguish between and study the different EV subpopulations. Despite the

lower secretion of IEVs compared to sEVs in 3T3-L1 adipocytes, a larger diversity of proteins was identified in the IEV fractions, dissociating the amount of EVs secreted per cell and their quality (referring to their protein signature). The many more unique proteins in IEVs may simply be related to the highest ability of large vesicles to encompass more material, especially cytosolic proteins, as illustrated by the numerous enzymes recovered in the IEV fractions. Another plausible explanation may rely on the specific sorting of exosomes from MVBs, which is known to be controlled by Rab GTPases and other ESCRT proteins [51,52], therefore leading to the engulfment of a restricted number of proteins in sEVs. Nonetheless, we cannot rule out that such specific sorting processes also exist for microvesicles, since the Rho family of small GTPases has also been involved in microvesicle shedding in response to different stimuli [53–55].

Identification of selective markers of EV subsets constitutes a critical issue to distinguish between the shared and specific functional properties of IEVs and sEVs. We first confirmed by Western blot a specific enrichment of sEVs in the exosomal markers Alix, TSG101 and tetraspanins (CD9, CD63 and CD81). However, tetraspanins (with the exception of CD81) were not detected in the quantitative proteomic analysis of EVs, probably because of their membrane-anchored nature. Nevertheless, proteomic profiling between IEVs and sEVs enabled us to identify new potential protein markers for large and small vesicles, confirmed by Western blotting, based on their selective presence or enrichment in one of these two EV subtypes. We identified  $\beta$ -actin specifically in IEVs and confirmed the enrichment of IEVs with endoplasmic (also called gp96) and actinin-4, as recently reported [41,42]. By contrast, we identified MVP to be specifically enriched in sEVs, whereas it has recently been shown to preferentially associate with IEV subsets [41]. Similarly, syntenin-1, shown to be highly specific to the light sEVs in the same study [41], was, in our experimental conditions, equally distributed between IEVs and sEVs. These discrepancies could be explained by: (i) the EV-producing cell model (adipocytes vs dendritic cells), which may express differently the proteins concerned; and/or (ii) the isolation procedure for IEVs, which differ since we pelleted IEVs at  $15,000 \times g$  (whereas others used  $10,000 \times g$  centrifugation, leading to the co-isolation of part of our IEVs in their exosomal preparations). Such results underline the necessity of using a combination of different protein markers to face and overcome the differences between cell models.

One approach to categorising EV subsets may be to combine different analyses including their lipid

contents. From this perspective, we performed a quantitative lipidomic analysis of IEVs and sEVs to assess the specific lipid characteristics of these two EV categories. Similar PL profiles were obtained for IEVs and sEVs, which confirms the high enrichment of EVs in SM and PC lipid classes [11,56]. Despite no quantitative changes in the different lipid classes between the two EV subsets, we highlighted a high proportion of externalised PS in IEVs and a specific enrichment of cholesterol in sEV preparations. These subtle changes were not evidenced in the lipidomic analysis performed by MS, but only detected following additional analysis of EV samples by flow cytometry, for testing annexin V positivity, and by the quantification of cholesterol content following colorimetric assay. A high proportion of sterols, relative to total PLs, has already been shown to be a specific trait of exosomes [56], which may be related to a particular enrichment of lipid-raft-like domains in this EV population [57]. In addition, annexin V positivity is a biological parameter often associated with the characterisation of IEVs, particularly in the cardiovascular field, since it predicts the pro-coagulant potential of this EV subclass [58]. Altogether, our results argue for the use of these lipid characteristics, in addition to morphometric and biochemical parameters, since it can help to categorise EV subtypes and may also influence intrinsic EV properties.

So far, all of the studies investigating adipocyte-derived EVs have focused on exosomes [8,9,11,21]. Notably, adipose tissue-derived exosomes are increased in the context of obesity both in animal models [8] and in humans [21]. Enhanced circulating levels of total microvesicles and exosomes have been detected in obese patients [2,3,5], suggesting that adipocyte-derived EVs may contribute to such an increase. We confirmed the association of two specific adipose proteins (ap2/FABP4 and adiponectin) on EVs, as previously described [12–14], and their respective enrichment on either IEVs (for ap2/FABP4) or sEVs (for adiponectin). Such results highlight their potential to be used to characterise and evaluate the biodistribution of adipocyte-derived EV subclasses from body fluids.

In agreement with a potential role of adipocyte-derived EVs in metabolic complications associated with obesity, we observed an increase in adipocyte-derived EV secretion following stimulation with the calcium ionophore ionomycin, elevated PA and exposure to TNF $\alpha$ . These biological stimuli have all been associated with increased fat mass, and constitute critical signals in the myriad of cellular and subcellular dysfunctional networks associated with metabolic diseases in the context of obesity [43,59]. In particular, PA appears to be a potent

inducer of both lEV and sEV secretion. Increased plasma levels of free fatty acids, such as PA, occur in states of obesity and are proposed to play an important role in the development of insulin resistance, notably through the formation of ceramides and their pro-inflammatory-induced responses [60]. *De novo* synthesis of ceramides from PA has also been shown to regulate the inward budding of MVBs [61] and, accordingly, to enhance sEV secretion from adipocytes [10,62] and from skeletal muscle cells [22]. Nevertheless, the so-called “exosomes” fraction may contain lEVs, depending on the isolation procedure used. Previous work has shown that exosomes are likely to transfer the deleterious effect of PA between muscle cells, thereby participating in the alteration of muscle homeostasis following lipid-induced insulin resistance in mice [22]. In the light of our study, it would be necessary to reconsider all EV populations as potential carriers of lipids related to diet-induced changes in fatty acid composition, which may play important roles in the deleterious effects of lipid-induced insulin resistance at the level of the whole organism.

EVs are now recognised as biological vectors of cellular communication. Our quantitative proteomic analysis of adipocyte-derived EVs revealed that lEV and sEV subpopulations present specific signatures, which may reflect different biological and functional properties on recipient cells and tissues. Studies investigating the functional responses of adipocyte-derived exosomes have revealed their ability to modulate macrophage activation [8], insulin response [7] and even tumorigenicity [21]. In the light of our study, showing that lEVs carry many proteins from diverse origins and are specifically enriched in metabolic enzymes (mainly of mitochondrial origin), one can advance the hypothesis that they may modulate metabolic pathways in recipient cells, such as fatty acid oxidation, a feature already attributed to adipocyte exosomes [21]. Moreover, high annexin V binding of adipocyte-derived lEVs could predict specific pro-coagulant properties of this fat cell EV subtype, in agreement with the detection of tissue factor proteins only in the lEV fractions (see Dataset S2), and may participate in the cardiovascular complications associated with obesity. Therefore, our results highlight the need to distinguish adipocyte-derived subtypes to delineate their respective functional properties.

Altogether, this study provides additional information and clues to characterise and define EV subtypes based on the characterisation of adipocyte-derived EV populations. From a more general perspective, it illustrates the need for a combination of multiple techniques to appreciate the complexity of EV subtypes before investigating their functional roles.

## Acknowledgements

We thank Dr J Pairault for providing 3T3-L1 cells, and Dr Isabelle Dugail (INSERM UMRS 1166, team 6 Nutriomics, Hôpital La Pitié Salpêtrière, Paris) and Dr Pascale Zimmerman (Centre de recherche en cancérologie de Marseille and University Leuven) for generous gifts of antibodies. We thank Dr J-C Gimel for providing access to NTA technology and for helpful discussion regarding the analysis of the results.

## Disclosure statement

No potential conflict of interest was reported by the authors.

## Funding

This work was supported by the French National Research Agency through the program MilkChEST no. ANR-12-BSV6-0013-04, GIS APIS-GENE, by a regional grant from Région Pays de la Loire and by a research grant from Société Francophone du Diabète (SFD). MD is funded by a Ph.D. fellowship from the French research ministry and AF is financed by a Ph.D. fellowship from Région Pays de la Loire.

## References

- [1] Stern JH, Rutkowski JM, Scherer PE. Adiponectin, leptin, and fatty acids in the maintenance of metabolic homeostasis through adipose tissue crosstalk. *Cell Metab.* 2016;23(5):770–784.
- [2] Goichot B, Grunebaum L, Desprez D, et al. Circulating procoagulant microparticles in obesity. *Diabetes Metab.* 2006;32(1):82–85.
- [3] Stepanian A, Bourguignat L, Hennou S, et al. Microparticle increase in severe obesity: not related to metabolic syndrome and unchanged after massive weight loss. *Obesity (Silver Spring).* 2013;21(11):2236–2243.
- [4] Agouni A, Lagrue-Lak-Hal AH, Ducluzeau PH, et al. Endothelial dysfunction caused by circulating microparticles from patients with metabolic syndrome. *Am J Pathol.* 2008;173(4):1210–1219.
- [5] Kranendonk ME, de Kleijn DP, Kalkhoven E, et al. Extracellular vesicle markers in relation to obesity and metabolic complications in patients with manifest cardiovascular disease. *Cardiovasc Diabetol.* 2014;13:37.
- [6] Kranendonk ME, Visseren FL, van Balkom BW, et al. Human adipocyte extracellular vesicles in reciprocal signaling between adipocytes and macrophages. *Obesity (Silver Spring).* 2014;22(5):1296–1308.
- [7] Kranendonk ME, Visseren FL, van Herwaarden JA, et al. Effect of extracellular vesicles of human adipose tissue on insulin signaling in liver and muscle cells. *Obesity (Silver Spring).* 2014;22(10):2216–2223.
- [8] Deng ZB, Poliakov A, Hardy RW, et al. Adipose tissue exosome-like vesicles mediate activation of macrophage-induced insulin resistance. *Diabetes.* 2009;58(11):2498–2505.

- [9] Lee JE, Moon PG, Lee IK, et al. Proteomic analysis of extracellular vesicles released by adipocytes of Otsuka Long-Evans Tokushima fatty (OLETF) rats. *Protein J*. 2015;34(3):220–235.
- [10] Müller G, Schneider M, Biemer-Daub G, et al. Microvesicles released from rat adipocytes and harboring glycosylphosphatidylinositol-anchored proteins transfer RNA stimulating lipid synthesis. *Cell Signal*. 2011;23(7):1207–1223.
- [11] Connolly KD, Guschina IA, Yeung V, et al. Characterisation of adipocyte-derived extracellular vesicles released pre- and post-adipogenesis. *J Extracellular Vesicles*. 2015;4:29159.
- [12] DeClercq V, d'Eon B, McLeod RS. Fatty acids increase adiponectin secretion through both classical and exosome pathways. *Biochim Biophys Acta*. 2015;1851(9):1123–1133.
- [13] Kralisch S, Klötting N, Ebert T, et al. Circulating adipocyte fatty acid-binding protein induces insulin resistance in mice in vivo. *Obesity (Silver Spring)*. 2015;23(5):1007–1013.
- [14] Ertunc ME, Sikkeland J, Fenaroli F, et al. Secretion of fatty acid binding protein aP2 from adipocytes through a nonclassical pathway in response to adipocyte lipase activity. *J Lipid Res*. 2015;56(2):423–434.
- [15] Phoonsawat W, Aoki-Yoshida A, Tsuruta T, et al. Adiponectin is partially associated with exosomes in mouse serum. *Biochem Biophys Res Commun*. 2014;448(3):261–266.
- [16] Colombo M, Raposo G, Théry C. Biogenesis, secretion, and intercellular interactions of exosomes and other extracellular vesicles. *Annu Rev Cell Dev Biol*. 2014;30:255–289.
- [17] Morel O, Jesel L, Freyssinet JM, et al. Cellular mechanisms underlying the formation of circulating microparticles. *Arterioscler Thromb Vasc Biol*. 2011;31(1):15–26.
- [18] Kunzelmann-Marche C, Freyssinet JM, Martinez MC. Regulation of phosphatidylserine transbilayer redistribution by store-operated Ca<sup>2+</sup> entry: role of actin cytoskeleton. *J Biol Chem*. 2001;276(7):5134–5139.
- [19] Bobrie A, Colombo M, Krumeich S, et al. Diverse subpopulations of vesicles secreted by different intracellular mechanisms are present in exosome preparations obtained by differential ultracentrifugation. *J Extracellular Vesicles*. 2012;1.
- [20] Lotvall J, Hill AF, Hochberg F, et al. Minimal experimental requirements for definition of extracellular vesicles and their functions: a position statement from the International Society for Extracellular Vesicles. *J Extracellular Vesicles*. 2014;3:26913.
- [21] Lazar I, Clement E, Dauvillier S, et al. Adipocyte exosomes promote melanoma aggressiveness through fatty acid oxidation: a novel mechanism linking obesity and cancer. *Cancer Res*. 2016;76(14):4051–4057.
- [22] Aswad H, Forterre A, Wiklander OP, et al. Exosomes participate in the alteration of muscle homeostasis during lipid-induced insulin resistance in mice. *Diabetologia*. 2014;57(10):2155–2164.
- [23] Fleury A, Hoch L, Martinez MC, et al. Hedgehog associated to microparticles inhibits adipocyte differentiation via a non-canonical pathway. *Sci Rep*. 2016;6:23479.
- [24] Rodbell M. Metabolism of isolated fat cells. I. Effects of hormones on glucose metabolism and lipolysis. *J Biol Chem*. 1964;239:375–380.
- [25] Fine JB, DiGirolamo M. A simple method to predict cellular density in adipocyte metabolic incubations. *Int J Obes Relat Metab Disord*. 1997;21(9):764–768.
- [26] Zonneveld MI, Brisson AR, van Herwijnen MJ, et al. Recovery of extracellular vesicles from human breast milk is influenced by sample collection and vesicle isolation procedures. *J Extracellular Vesicles*. 2014;3.
- [27] Shevchenko A, Wilm M, Vorm O, et al. Mass spectrometric sequencing of proteins silver-stained polyacrylamide gels. *Anal Chem*. 1996;68(5):850–858.
- [28] Liu H, Sadygov RG, Yates JR 3rd. A model for random sampling and estimation of relative protein abundance in shotgun proteomics. *Anal Chem*. 2004;76(14):4193–4201.
- [29] Chelius D, Bondarenko PV. Quantitative profiling of proteins in complex mixtures using liquid chromatography and mass spectrometry. *J Proteome Res*. 2002;1(4):317–323.
- [30] Valot B, Langella O, Nano E, et al. MassChroQ: a versatile tool for mass spectrometry quantification. *Proteomics*. 2011;11(17):3572–3577.
- [31] Team RC. R: A language and environment for statistical computing. Vienna (Austria): R Foundation for Statistical Computing; 2014. Available from: <http://www.R-project.org/>
- [32] Matyash V, Liebisch G, Kurzchalia TV, et al. Lipid extraction by methyl-tert-butyl ether for high-throughput lipidomics. *J Lipid Res*. 2008;49(5):1137–1146.
- [33] Fauland A, Köfeler H, Trötz Müller M, et al. A comprehensive method for lipid profiling by liquid chromatography-ion cyclotron resonance mass spectrometry. *J Lipid Res*. 2011;52(12):2314–2322.
- [34] Hartler J, Trötz Müller M, Chitruju C, et al. Lipid Data Analyzer: unattended identification and quantitation of lipids in LC-MS data. *Bioinformatics*. 2011;27(4):572–577.
- [35] Théry C, Boussac M, Véron P, et al. Proteomic analysis of dendritic cell-derived exosomes: a secreted subcellular compartment distinct from apoptotic vesicles. *J Immunol*. 2001;166(12):7309–7318.
- [36] Théry C, Amigorena S, Raposo G, et al. Isolation and characterization of exosomes from cell culture supernatants and biological fluids. *Curr Protoc Cell Biol*. 2006: Chapter 3:Unit 3.22.1-3.22.9
- [37] Fox JE, Austin CD, Boyles JK, et al. Role of the membrane skeleton in preventing the shedding of procoagulant-rich microvesicles from the platelet plasma membrane. *J Cell Biol*. 1990;111(2):483–493.
- [38] Théry C, Ostrowski M, Segura E. Membrane vesicles as conveyors of immune responses. *Nat Rev Immunol*. 2009;9(8):581–593.
- [39] Wang G, Wu WW, Zeng W, et al. Label-free protein quantification using LC-coupled ion trap or FT mass spectrometry: reproducibility, linearity, and application with complex proteomes. *J Proteome Res*. 2006;5(5):1214–1223.
- [40] Ono M, Shitashige M, Honda K, et al. Label-free quantitative proteomics using large peptide data sets generated by nanoflow liquid chromatography and mass

- spectrometry. *Mol Cell Proteomics*. 2006;5(7):1338–1347.
- [41] Kowal J, Arras G, Colombo M, et al. Proteomic comparison defines novel markers to characterize heterogeneous populations of extracellular vesicle subtypes. *Proc Natl Acad Sci U S A*. 2016;113(8):E968–77.
- [42] Willms E, Johansson HJ, Mäger I, et al. Cells release subpopulations of exosomes with distinct molecular and biological properties. *Sci Rep*. 2016;6:22519.
- [43] Arruda AP, Hotamisligil GS. Calcium homeostasis and organellar function in the pathogenesis of obesity and diabetes. *Cell Metab*. 2015;22(3):381–397.
- [44] Ailhaud G, Fukamizu A, Massiera F, et al. Angiotensinogen, angiotensin II and adipose tissue development. *Int J Obes Relat Metab Disord*. 2000;24(Suppl 4):S33–5.
- [45] Ouchi N, Parker JL, Lugus JJ, et al. Adipokines in inflammation and metabolic disease. *Nat Rev Immunol*. 2011;11(2):85–97.
- [46] Pasquet JM, Dachary-Prigent J, Nurden AT. Calcium influx is a determining factor of calpain activation and microparticle formation in platelets. *Eur J Biochem*. 1996;239(3):647–654.
- [47] Raposo G, Tenza D, Mecheri S, et al. Accumulation of major histocompatibility complex class II molecules in mast cell secretory granules and their release upon degranulation. *Mol Biol Cell*. 1997;8(12):2631–2645.
- [48] Burger D, Montezano AC, Nishigaki N, et al. Endothelial microparticle formation by angiotensin II is mediated via Ang II receptor type I/NADPH oxidase/Rho kinase pathways targeted to lipid rafts. *Arterioscler Thromb Vasc Biol*. 2011;31(8):1898–1907.
- [49] van Niel G, Raposo G, Candalh C, et al. Intestinal epithelial cells secrete exosome-like vesicles. *Gastroenterology*. 2001;121(2):337–349.
- [50] Combes V, Simon AC, Grau GE, et al. In vitro generation of endothelial microparticles and possible prothrombotic activity in patients with lupus anticoagulant. *J Clin Invest*. 1999;104(1):93–102.
- [51] Ostrowski M, Carmo NB, Krumeich S, et al. Rab27a and Rab27b control different steps of the exosome secretion pathway. *Nat Cell Biol*. 2010;121:19–30. sup pp 1–13.
- [52] Colombo M, Moita C, van Niel G, et al. Analysis of ESCRT functions in exosome biogenesis, composition and secretion highlights the heterogeneity of extracellular vesicles. *J Cell Sci*. 2013;126(Pt 24):5553–5565.
- [53] Sapet C, Simoncini S, Loriod B, et al. Thrombin-induced endothelial microparticle generation: identification of a novel pathway involving ROCK-II activation by caspase-2. *Blood*. 2006;108(6):1868–1876.
- [54] Muralidharan-Chari V, Clancy J, Plou C, et al. ARF6-regulated shedding of tumor cell-derived plasma membrane microvesicles. *Curr Biol*. 2009;19(22):1875–1885.
- [55] Antonyak MA, Wilson KF, Cerione RA. R(h)oads to microvesicles. *Small Gtpases*. 2012;3(4):219–224.
- [56] Llorente A, Skotland T, Sylväne T, et al. Molecular lipidomics of exosomes released by PC-3 prostate cancer cells. *Biochim Biophys Acta*. 2013;1831(7):1302–1309.
- [57] de Gassart A, Geminard C, Fevrier B, et al. Lipid raft-associated protein sorting in exosomes. *Blood*. 2003;102(13):4336–4344.
- [58] Sims PJ, Wiedmer T, Esmon CT, et al. Assembly of the platelet prothrombinase complex is linked to vesiculation of the platelet plasma membrane. Studies in Scott syndrome: an isolated defect in platelet procoagulant activity. *J Biol Chem*. 1989;264(29):17049–17057.
- [59] Gregor MF, Hotamisligil GS. Inflammatory mechanisms in obesity. *Annu Rev Immunol*. 2011;29:415–445.
- [60] Holland WL, Bikman BT, Wang LP, et al. Lipid-induced insulin resistance mediated by the proinflammatory receptor TLR4 requires saturated fatty acid-induced ceramide biosynthesis in mice. *J Clin Invest*. 2011;121(5):1858–1870.
- [61] Trajkovic K, Hsu C, Chiantia S, et al. Ceramide triggers budding of exosome vesicles into multivesicular endosomes. *Science*. 2008;319(5867):1244–1247.
- [62] Eguchi A, Mulya A, Lazic M, et al. Microparticles release by adipocytes act as “find-me” signals to promote macrophage migration. *Plos One*. 2015;10(4):e0123110.